



저작자표시-비영리-변경금지 2.0 대한민국

이용자는 아래의 조건을 따르는 경우에 한하여 자유롭게

- 이 저작물을 복제, 배포, 전송, 전시, 공연 및 방송할 수 있습니다.

다음과 같은 조건을 따라야 합니다:



저작자표시. 귀하는 원저작자를 표시하여야 합니다.



비영리. 귀하는 이 저작물을 영리 목적으로 이용할 수 없습니다.



변경금지. 귀하는 이 저작물을 개작, 변형 또는 가공할 수 없습니다.

- 귀하는, 이 저작물의 재이용이나 배포의 경우, 이 저작물에 적용된 이용허락조건을 명확하게 나타내어야 합니다.
- 저작권자로부터 별도의 허가를 받으면 이러한 조건들은 적용되지 않습니다.

저작권법에 따른 이용자의 권리는 위의 내용에 의하여 영향을 받지 않습니다.

이것은 [이용허락규약\(Legal Code\)](#)을 이해하기 쉽게 요약한 것입니다.

[Disclaimer](#)

The role of gelsolin and novel noncoding  
RNAs on the regulation of proinflammatory  
cytokines and tumor progression

Jiyeon Lee

Department of Medical Science  
The Graduate School, Yonsei University

The role of gelsolin and novel noncoding  
RNAs on the regulation of proinflammatory  
cytokines and tumor progression

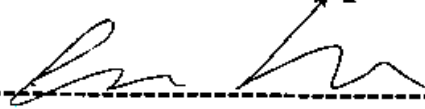
Directed by Professor Lark Kyun Kim

The Doctoral Dissertation  
submitted to the Department of Medical Science,  
the Graduate School of Yonsei University  
in partial fulfillment of the requirements for the degree of  
Doctor of Philosophy in Medical Science

Jiyeon Lee

December 2023

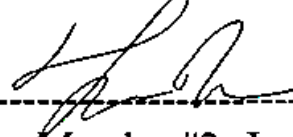
This certifies that the Doctoral Dissertation of  
Jiyeon Lee is approved.



Thesis Supervisor: Lark Kyun Kim



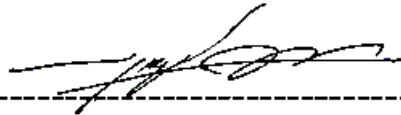
Thesis Committee Member#1: Jeon-Soo Shin



Thesis Committee Member#2: Je-Wook Yu



Thesis Committee Member#3: Ji-Hwan Ryu



Thesis Committee Member#4: Yong-ho Lee

The Graduate School  
Yonsei University

December 2023

## ACKNOWLEDGEMENTS

I am deeply grateful to Prof. Lark Kyun Kim for being my guiding light throughout my academic journey, offering me numerous opportunities for research. I want to express my heartfelt appreciation for the invaluable role you played in fostering my growth as a scientist. Thank you sincerely.

I would like to express my gratitude to Prof. Rimpei Morita of Nippon Medical School and the members of his lab for their significant contributions and support in the research included in this thesis. I am also thankful to Prof. Sun Shim Choi of Kangwon National University and Prof. Jungmin Choi of Korea University for their guidance and assistance.

I am grateful to Prof. Jeon-Soo Shin, Prof. Je-Wook Yu, Prof. Ji-Hwan Ryu, Prof. Yong-Ho Lee, the Committee members, for invaluable advice and guidance, helping me successfully complete my degree. Your support and encouragement have been greatly appreciated.

Additionally, I would like to express my gratitude to the members of Prof. Lark Kyun Kim's lab, including Dr. So Hee Dho.

Lastly, I want to express my gratitude to my dear mother, who always supports and empowers me, and to my friends who bring joy to my life.

## <TABLE OF CONTENTS>

ABSTRACT.....	vi
I. INTRODUCTION .....	1
1. Regulation of IL-1 $\beta$ expression: Gelsolin-mediated negative modulation of NLRP3 inflammasome activation .....	1
2. Regulation of TNF $\alpha$ expression: Unveiling the role of hypersensitive site-9 enhancer RNA in <i>Tnf</i> gene control.....	3
3. Alternative role of noncoding RNAs: Involvement in tumor progression ...	5
II. MATERIALS AND METHODS .....	7
1. Assays for immunological research.....	7
A. Mice .....	7
B. Cell culture and stimulation .....	7
C. Plasmid construction and transfection .....	8
D. Antisense oligonucleotides design and transfection .....	8
E. Co-immunoprecipitation .....	9
F. Gel filtration chromatography.....	9
G. Immunoblot analysis .....	9
H. ELISA .....	10
I. RNA isolation and Quantitative real-time PCR .....	11
J. Cytotoxicity assay .....	11
K. ASC oligomerization assay.....	12
L. Reconstitution of NLRP3 inflammasome system in HEK293T cells ....	12
M. Subcellular Fractionation .....	12
N. Measurement of intracellular calcium .....	12
O. Mitochondrial function assays .....	13
P. Transmission electron microscopy .....	13
Q. Flow cytometry .....	14

R. Immunofluorescence cell staining	14
S. MSU-induced peritonitis	15
T. LPS-induced septic shock	15
2. Assays for cancer research	15
A. Cell culture and transfection	15
B. RNA isolation and quantitative real-time PCR	16
C. Cell counting kit-8 assay	16
D. IncuCyte® cell proliferation assay	17
E. Colony formation assay	17
F. Invasion and migration assays	17
G. Wound-healing assay	17
III. RESULTS	19
1. Regulation of IL-1 $\beta$ expression: Gelsolin-mediated negative modulation of NLRP3 inflammasome activation	19
A. Gelsolin binds to NLRP3 at the priming step	19
B. Gelsolin negatively regulates NLRP3 inflammasome activation and pyroptosis	23
C. Gelsolin inhibits the translocation of NLRP3 to mitochondria during the priming process by disturbing the association between NLRP3 and a mitochondrial protein MAVS	30
D. Gelsolin serves as a reservoir for calcium and maintains mitochondrial stability	34
E. Gelsolin inhibits NLRP3 inflammasome activation <i>in vivo</i>	40
2. Regulation of TNF $\alpha$ expression: Unveiling the role of hypersensitive site-9 enhancer RNA in <i>Tnf</i> gene control	44
A. Downregulation of hypersensitive site-9 eRNA reduces TNF $\alpha$ expression	44
B. Deletion of hypersensitive site-9 region reduces TNF $\alpha$ expression	47

3. Alternative role of noncoding RNAs: Involvement in tumor progression ..	51
A. Selection of antisense oligonucleotides for the precise knockdown of the eRNA <i>THUMPD3-AS1</i> and <i>LINC01572</i> , and the lncRNA <i>PLEKHA8P1</i> in HCC cell line.....	51
B. The eRNA <i>THUMPD3-AS1</i> and <i>LINC01572</i> , and the lncRNA <i>PLEKHA8P1</i> promotes proliferation, invasion, and migration in HCC cells .....	53
IV. DISCUSSION .....	57
1. Regulation of IL-1 $\beta$ expression: Gelsolin-mediated negative modulation of NLRP3 inflammasome activation .....	57
2. Regulation of TNF $\alpha$ expression: Unveiling the role of hypersensitive site-9 enhancer RNA in <i>Tnf</i> gene control.....	59
3. Alternative role of noncoding RNAs: Involvement in tumor progression ..	60
V. CONCLUSION .....	61
REFERENCES .....	62
ABSTRACT(IN KOREAN) .....	70
PUBLICATION LIST .....	72

## LIST OF FIGURES

Figure 1. Gelsolin interacts with NLRP3 in LPS-primed macrophages .....	21
Figure 2. Gelsolin deficiency results in excessive NLRP3 inflammasome activation.....	25
Figure 3. Gelsolin does not affect the NF- $\kappa$ B pathway .....	27
Figure 4. Gelsolin deficiency promotes pyroptotic cell death .....	28
Figure 5. Gelsolin depletion promotes the translocation of NLRP3 to mitochondria.....	32
Figure 6. Gelsolin inhibits the association between NLRP3 and MAVS .....	33
Figure 7. The association between gelsolin and NLRP3 is dependent on calcium.....	36
Figure 8. Intracellular calcium concentration is increased in the absence of gelsolin .....	37
Figure 9. Ablation of gelsolin promotes mitochondrial dysfunction	38
Figure 10. Gelsolin deficiency aggravates the immunopathologic responses in the MSU-induced peritonitis model .....	41
Figure 11. Gelsolin deficiency aggravates the immunopathologic responses in the LPS-induced septic shock model .....	42
Figure 12. A graphic summary of the mechanism of gelsolin negatively regulating NLRP3 .....	43
Figure 13. ASO-mediated knockdown of HSS-9 eRNA in mouse	

BMDMs .....	45
Figure 14. Knockdown of HSS-9 eRNA reduces TNF $\alpha$ expression in macrophages .....	46
Figure 15. No expression of HSS-9 eRNA in HSS-9-KO BMDMs ..	48
Figure 16. Deletion of HSS-9 reduces the expression of TNF $\alpha$ in macrophages .....	49
Figure 17. Deletion of HSS-9 reduces the expression of TNF $\alpha$ in the LPS-induced septic shock model .....	50
Figure 18. ASO-mediated knockdown of <i>PLEKHA8P1</i> in HCC cells .....	52
Figure 19. Downregulation of <i>THUMPD3-AS1</i> , <i>LINC01572</i> or <i>PLEKHA8P1</i> inhibits proliferation of HCC cells .....	54
Figure 20. Downregulation of <i>THUMPD3-AS1</i> , <i>LINC01572</i> or <i>PLEKHA8P1</i> inhibits migration and invasion of HCC cells .....	55

## ABSTRACT

**The role of gelsolin and novel noncoding RNAs on the regulation of proinflammatory cytokines and tumor progression**

Jiyeon Lee

*Department of Medical Science  
The Graduate School, Yonsei University*

(Directed by Professor Lark Kyun Kim)

Inflammatory diseases are often characterized by the excessive secretion of proinflammatory cytokines, such as IL-1 $\beta$  and TNF $\alpha$ , which serve as critical mediators in promoting inflammatory responses.

The release of IL-1 $\beta$  is tightly controlled by the NLRP3 inflammasome, a crucial component of the innate immune system. In this research, I identified gelsolin, a NLRP3 binding protein, as a negative regulator of NLRP3 inflammasome activation and, consequently, IL-1 $\beta$  expression. Knockout of gelsolin markedly enhances the NLRP3 inflammasome activation. Gelsolin hindered the translocation of NLRP3 to the mitochondria; it helped maintain the concentration of intracellular calcium and ultimately suppressed NLRP3 inflammasome. Therefore, gelsolin is a potential therapeutic target for the treatment of NLRP3-associated diseases.

Additionally, I discovered that TNF $\alpha$ , another important cytokine, is regulated by a novel enhancer RNA (eRNA) belonging to the class of noncoding RNAs (ncRNAs). Knockdown of hypersensitive site (HSS)-9 eRNA results in reduced TNF $\alpha$  levels. Deletion of *Tnf* HSS-9 region, where HSS-9 eRNA is transcribed, further decreases TNF $\alpha$  levels. This reduction in TNF $\alpha$  expression was observed in both serum and peritoneal fluid in the

LPS-induced sepsis mouse model, suggesting a potential protective effect against LPS-induced sepsis. This indicates that HSS-9 eRNA could be a promising therapeutic target for immune disorders involving TNF $\alpha$ .

Finally, I extended my research to explore the influence of ncRNAs on tumor progression. I uncovered that three novel ncRNAs, *THUMPD3-AS1*, *LINC01572*, and *PLEKHA8P1*, exhibited an oncogenic role in hepatocellular carcinoma (HCC). Knockdown of these three ncRNAs suppresses the proliferation, invasion, and migration of HCC cells, highlighting their potential as therapeutic targets for HCC treatment.

My study demonstrated novel regulatory mechanisms governing IL-1 $\beta$  and TNF $\alpha$ , and additionally demonstrated the role of ncRNAs in modulating TNF $\alpha$  expression and tumor progression. These findings propose new therapeutic strategies for inflammatory diseases and HCC.

---

Key words : proinflammatory cytokines, IL-1 $\beta$ , TNF $\alpha$ , gelsolin, NLRP3 inflammasome, ncRNAs, tumor progression, antisense oligonucleotides

## **The role of gelsolin and novel noncoding RNAs on the regulation of proinflammatory cytokines and tumor progression**

Jiyeon Lee

*Department of of Medical Science  
The Graduate School, Yonsei University*

(Directed by Professor Lark Kyun Kim)

### **I. INTRODUCTION**

#### **1. Regulation of IL-1 $\beta$ expression: Gelsolin-mediated negative modulation of NLRP3 inflammasome activation**

IL-1 $\beta$  plays a central role in autoinflammatory diseases, acting as a potent self-activator and triggering further autoinflammatory responses<sup>1</sup>. The maturation and secretion of IL-1 $\beta$  are tightly regulated by inflammasomes, which are multimeric cytosolic protein complexes<sup>1,2</sup>. Among the various inflammasomes, the NLRP3 inflammasome is the most extensively studied and consists of the sensor protein NLRP3, the adaptor protein ASC, and the effector protein pro-caspase-1<sup>2,3,4,5</sup>. Activation of the NLRP3 inflammasome occurs in two steps. In resting macrophages, pro-IL-1 $\beta$  and NLRP3 are either not expressed or expressed at insufficient levels for NLRP3 inflammasome activation. Pattern recognition receptors (PRRs) like Toll-like receptors (TLRs) recognize extracellular stimuli such as lipopolysaccharide (LPS) and upregulate the expression of pro-IL-1 $\beta$  and NLRP3 through NF- $\kappa$ B signaling<sup>3,4</sup>. To produce mature IL-1 $\beta$ , various stimuli, including bacterial toxin nigericin, extracellular ATP, and crystalline particles such as cholesterol crystals and monosodium urate (MSU) crystals, induce the formation of NLRP3, ASC and pro-caspase-1<sup>6</sup>. Upon activation, pro-caspase-1 undergoes autocleavage, leading to the conversion of

pro-IL-1 $\beta$  into biologically active IL-1 $\beta$  through the proteolytic activity of caspase-1. Additionally, active caspase-1 triggers an inflammatory form of cell death known as pyroptosis by cleaving the pore-forming protein Gasdermin D (GSDMD), which resulting in the release of IL-1 $\beta$ <sup>4,5</sup>.

The activation of the NLRP3 inflammasome leading to the systemic elevation of IL-1 $\beta$ , has been implicated in various chronic diseases such as Alzheimer's and Parkinson's disease, as well as metabolic disorders such as atherosclerosis, type 2 diabetes, obesity, and gout<sup>2,4</sup>. While numerous studies have focused on post-inflammasome activation regulation or the identification of inducers for inflammasome activation, fewer have investigated the modulation of NLRP3 prior to activation. For instance, it has been shown that LRRFIP2 can negatively regulate NLRP3 by binding to it after LPS priming and ATP stimulation<sup>7</sup>. Additionally, UCP1 KO mice exhibit increased NLRP3 inflammasome activation, which leads to the development of atherosclerosis when fed a high-fat diet<sup>8</sup>. Acidic mammalian chitinase (AMCase), an enzyme responsible for chitin degradation, has been found to promote caspase-1 activation<sup>9</sup>. Furthermore, mitochondrial ROS (mROS) has been shown to trigger lysosomal damage, thereby activating the NLRP3 inflammasome<sup>10,11</sup>.

NLRP3 can be constitutively primed by various mechanisms, with aging influencing its susceptibility to activation<sup>12</sup>. While specific signals like MSU, silica, or Amyloid- $\beta$  can activate the NLRP3 inflammasome<sup>13-15</sup>, controlling the expression or activity of NLRP3 itself before secondary stimulation can effectively prevent excessive inflammasome activation. Despite the abundance of studies on inflammasome activation, fewer investigations have focused on the modulation of NLRP3 prior to activation. To explore this aspect, my co-worker performed immunoprecipitation-mass spectrometry (IP-MS) on LPS-primed mouse bone marrow-derived macrophages (BMDMs) to identify molecules that can modulate NLRP3 prior to activation.

Gelsolin, a protein with six conserved homologous domains, has primarily been recognized for its role as an actin-binding protein. It regulates actin dynamics by severing

and capping filamentous actin (F-actin) and sequestering actin monomers (G-actin)<sup>16,17</sup>. The actin-binding and -severing properties of gelsolin are influenced by various factors such as intracellular calcium concentration, intracellular pH, and phosphatidylinositol 4,5-bisphosphate (PIP<sub>2</sub>). Its main function involves severing and removing circulating actin filaments from damaged cells or tissues, thereby preventing inflammatory responses and pathophysiological consequences. Studies have reported a significant downregulation of gelsolin levels in trauma patients, likely due to its role in binding and scavenging actin in response to injury<sup>18,19</sup>. Gelsolin has also been implicated in the development of inflammatory diseases such as rheumatoid arthritis and Alzheimer's disease<sup>19-21</sup>. While there is limited research on the involvement of gelsolin in NLRP3 inflammasome activation, Flightless-I, a member of the gelsolin superfamily, has been shown to negatively regulate NLRP3 inflammasome activation by inhibiting caspase-1 activity<sup>7,22,23</sup>.

In this study, I have identified gelsolin as a negative regulator of NLRP3 inflammasome activation. My findings demonstrate that gelsolin interacts with NLRP3 during the priming step, which occurs prior to the assembly and activation of the NLRP3 inflammasome. This interaction effectively prevents the translocation of NLRP3 to the mitochondria and maintains the intracellular calcium levels below the threshold that could potentially damage the mitochondria. Furthermore, I have confirmed that gelsolin-deficient mice exhibit a significant increase in inflammation upon treatment with MSU or LPS. Therefore, my results unveil a novel mechanism underlying NLRP3 inflammasome activation and propose gelsolin as a promising therapeutic target for diseases associated with NLRP3 inflammasome dysfunction.

## **2. Regulation of TNF $\alpha$ expression: Unveiling the role of hypersensitive site-9 enhancer RNA in *Tnf* gene control**

TNF $\alpha$ , initially recognized as an anti-tumor agent that triggers necrotic cell death in tumors and inhibits tumor cell proliferation, is a proinflammatory cytokine produced by immune

cells<sup>24,25</sup>. TNF $\alpha$  is one of the genes that undergo transcription shortly after activation<sup>26</sup>. It is produced by a variety of cell types, such as monocytes, macrophages, T lymphocytes, B lymphocytes, and natural killer cells<sup>26,27</sup>. TNF $\alpha$  is associated with a wide range of inflammatory diseases. Dysregulation of TNF $\alpha$  can lead to the development of Rheumatoid arthritis, Psoriasis, or Inflammatory bowel disease (IBD)<sup>28,29</sup>. For the treatment of these diseases, TNF $\alpha$ -targeted therapy is utilized. Anti-TNF $\alpha$  monoclonal antibodies such as Infliximab, Adalimumab, Golimumab, and Certolizumab pegol are used for this purpose<sup>30,31</sup>.

DNase I hypersensitive sites (HSSs) are regions that are accessible to transcription factors, and as a result, they are closely associated with transcriptional activity. It was reported that *Tnf* HSS-9 (9 kb upstream of the *Tnf* gene) promotes TNF $\alpha$  transcription by acting as an enhancer<sup>32</sup>. Enhancers not only provide binding sites for trans-acting factors but also are accessed and transcribed themselves by RNA pol II, leading to the generation of noncoding RNAs (ncRNAs) called enhancer RNAs (eRNAs)<sup>33,34</sup>. Recent studies have highlighted the significant regulatory role of eRNAs in controlling adjacent gene expression, as depletion of these molecules has been associated with decreased expression levels of neighboring target genes<sup>35,36</sup>. As a result, researchers are actively investigating the effects of eRNAs on various human diseases, including immune disorders<sup>37-39</sup>.

In this study, I demonstrated that the HSS-9 eRNA transcribed from the *Tnf* HSS-9 region regulates TNF $\alpha$  expression. To establish the role of HSS-9 eRNA in controlling TNF $\alpha$  expression, I designed antisense oligonucleotides (ASOs) specifically targeting HSS-9 eRNA and conducted knockdown experiments. By inducing knockdown of HSS-9 eRNA using ASOs in mouse BMDM cells, I successfully observed a reduction in HSS-9 eRNA expression. Consequently, I observed a decrease in the transcription of TNF $\alpha$  mRNA and the secretion of TNF $\alpha$  protein. TNF $\alpha$  expression was further reduced in knockout mice with a partial deletion of the *Tnf* HSS-9 region, where HSS-9 eRNA is transcribed. In conclusion, my study establishes a novel regulatory mechanism for TNF $\alpha$  and highlights the potential therapeutic targeting of HSS-9 eRNA in the future.

### 3. Alternative role of noncoding RNAs: Involvement in tumor progression

The aberrant expression of eRNAs and long noncoding RNAs (lncRNAs), both classified as ncRNAs, is also associated with the dysregulation of oncogenes and tumor suppressor genes<sup>40,41</sup>.

Hepatocellular carcinoma (HCC) stands as the most prevalent type of primary liver cancer, presenting a considerable burden on global health<sup>42</sup>. The main approach to clinical management for HCC relies heavily on the Barcelona Clinic Liver Cancer (BCLC) staging classification<sup>43</sup>. Patients at early stages (BCLC stage 0-A) are typically advised to undergo potentially curative treatments such as surgical resection, liver transplantation, or tumor ablation<sup>44</sup>. For individuals at the intermediate stage (BCLC stage B), the standard treatment is transarterial chemoembolization (TACE)<sup>45</sup>. Advanced-stage patients (BCLC stage C) or those who encounter disease progression after TACE are administered systemic treatment.

Although there are well-established guidelines for various therapies, the difficulties in early detection and the widespread resistance to conventional treatments like chemotherapy<sup>43</sup>, have led to restricted treatment efficacy and unfavorable survival rates in HCC patients. With a 5-year survival rate of just 20%, HCC exhibits the second lowest survival rate among all types of cancer, second only to pancreatic cancer<sup>46</sup>. Consequently, extensive research efforts have been focused on identifying novel therapeutic targets. However, the specific roles of ncRNAs in HCC remain largely unknown, underscoring the need for further investigation in this area.

In this study, I have identified tumorigenic role of eRNAs *THUMPD3-AS1*, *LINC01572*, and lncRNAs *PLEKHA8P1*. I confirmed that knockdown of *THUMPD3-AS1*, *LINC01572*, or *PLEKHA8P1* using ASOs reduced the proliferation of FT3-7, the human HCC cell line. Furthermore, I observed that downregulation of these ncRNAs resulted in diminished migration and invasion abilities. My research therefore makes a valuable

contribution to the developing field of identifying and characterizing novel therapeutic ncRNAs that regulate tumor proliferation and metastasis.

## II. MATERIALS AND METHODS

### 1. Assays for immunological research

#### A. Mice

The C57BL/6 background *Gsn<sup>fl/fl</sup>* and *Gsn<sup>ΔMye</sup>* mice were kindly provided by Professor Rimpei Morita at Nippon Medical School. Mouse studies were conducted in accordance with protocols approved by the Department of Laboratory Animal Resources Ethical Committee of Yonsei University College of Medicine. All mice were housed under specific pathogen-free (SPF) conditions. Mice (6–10 weeks old) from the same cage were randomly selected for different treatments.

#### B. Cell culture and stimulation

To generate mouse BMDMs, bone marrow cells were flushed from the femurs and tibias of 6–10-week-old mice using DPBS. The cells were then cultured in Dulbecco's modified Eagle's medium (DMEM) supplemented with 10% FBS, 20% L929 cell-conditioned medium, and 100 U/mL-100 μg/mL penicillin-streptomycin for 7 days. Mouse peritoneal macrophages were obtained from the peritoneal cavity of 6–10-week-old mice and cultured in DMEM supplemented with 10% FBS and 100 U/mL-100 μg/mL penicillin-streptomycin.

The J774.1 mouse macrophage cell line was cultured in Roswell Park Memorial Institute (RPMI) 1640 supplemented with 10% FBS, 1 mM sodium pyruvate, 2 mM L-glutamine, 100 × MEM Non-Essential Amino Acids, 100 U/mL-100 μg/mL penicillin-streptomycin, and 50 μM 2-mercaptoethanol.

HEK293T, a human embryonic kidney cell line, was cultured in DMEM supplemented with 10% FBS and 100 U/mL-100 μg/mL penicillin-streptomycin.

For inflammasome activation, cells were primed with 500 ng/mL LPS-EK Ultrapure (Invivogen, San Diego, CA, USA) for 3 h, followed by stimulation with indicated

concentration of nigericin (Invivogen, San Diego, CA, USA) for the indicated duration of time.

### **C. Plasmid construction and transfection**

pcDNA3-N-Flag-NLRP3 was purchased from addgene (75127, Addgene, Watertown, MA, USA). DNA fragments encoding murine gelsolin, ASC, Pro-caspase-1, and MAVS were obtained by PCR-based amplification of cDNA from J774.1 cells and subcloned into pcDNA3-6 × Myc, pCS4-3 × HA, and pcDNA3.1/V5-His A, respectively. Truncated mutant constructs of NLRP3 and gelsolin were generated by subcloning the PCR products from plasmids expressing full-length NLRP3 and gelsolin into pcDNA3-N-Flag and pcDNA3-6 × Myc, respectively. The constructs were transiently transfected into HEK293T cells for 48 h using Lipofectamine 2000 (Invitrogen, Waltham, MA, USA) as per manufacturer's instructions. To chelate calcium, BAPTA-AM (Calbiochem, San Diego, CA, USA) at concentrations of 5 μM, 20 μM, and 40 μM was co-treated with the transfection.

### **D. Antisense oligonucleotides design and transfection**

ASOs used to knockdown HSS-9 eRNA were designed and purchased from Qiagen. A total of  $1 \times 10^6$  cells were electroporated with 500 nM ASO using Neon® Transfection System (Thermo Fisher Scientific, Waltham, MA, USA), following the manufacturer's instructions. The electroporation parameters used were 1400 V, 20 ms, and 2 pulses. Subsequently, the cells were immediately transferred to pre-warmed media without any antibiotics. After 48 h of transfection, the cells were treated with 100 ng/mL LPS for 1 h. Following the treatment, both the cells and the cell culture supernatant were collected for qRT-PCR and ELISA analysis. The ASO sequences are as follows: Negative control ASO: 5'-AACACGTCTATACGC-3', HSS-9 eRNA ASO 1: 5'-TTAGATTTGAG GTTAC-3', HSS-9 eRNA ASO 2: 5'-GGTTAAACTTGGGTAA-3', and HSS-9 eRNA ASO 3: 5'-GGGTGAAGGTAAACT-3'.

### **E. Co-immunoprecipitation (Co-IP)**

To perform Co-IP of overexpressed proteins in HEK293T cells, the cells were transfected with the indicated plasmids as described above and then lysed in ice-cold IP lysis buffer (50 mM HEPES, pH 7.0, 250 mM NaCl, 1 mM EDTA, 0.2% Nonidet P-40) containing a protease inhibitor cocktail (Bio-rad, Hercules, CA, USA). Cell lysates were collected after centrifugation at maximum speed for 15 min. The whole-cell lysates were then incubated with anti-Flag M2 affinity gel (Sigma, St. Louis, MO, USA) or anti-c-Myc agarose conjugate (Sigma, St. Louis, MO, USA) and rotated at 4 °C overnight. The beads were extensively washed three times with IP lysis buffer, and the immunoprecipitates were eluted from the beads with IP elution buffer (0.1 M glycine HCl, pH 3.5) and neutralized with IP neutralization buffer (0.5 M Tris HCl, pH 7.4, with 1.5 M NaCl). Both the whole-cell lysates and immunoprecipitates were subjected to immunoblot analysis.

### **F. Gel filtration chromatography**

BMDMs were primed with LPS and then stimulated with nigericin or left unstimulated. The cells were lysed in ice-cold NP-40 lysis buffer (50 mM Tris-HCl, pH 7.4, 1% NP-40, and 150 mM NaCl) containing a protease inhibitor cocktail (Bio-rad, Hercules, CA, USA), and centrifuged at maximum speed for 15 min. Fresh soluble lysate containing 2.5 mg of total protein was loaded onto an XK 16/70 column packed with superdex 200 prep grade resin (Cytiva, Marlborough, MA, USA). The proteins were fractionated using an ÄKTA Pure Protein Purification System (Cytiva, Marlborough, MA, USA) in a buffer containing 20 mM sodium phosphate and 150 mM NaCl at pH 7.0. Each 5 mL fraction was collected and concentrated using an Amicon ultra centrifugal filter, and the concentrated samples were subjected to immunoblot analysis.

### **G. Immunoblot analysis**

The cells were lysed in RIPA buffer (CST, Danvers, MA, USA) supplemented with a protease inhibitor cocktail (Bio-rad, Hercules, CA, USA). Whole-cell lysates were collected by centrifugation at maximum speed for 15 min and the protein concentrations

were quantified using the BCA assay (Pierce, Waltham, MA, USA). Equal amounts of protein were then separated by SDS-poly acrylamide gel electrophoresis (PAGE) and transferred onto nitrocellulose membranes. The membranes were probed with specific primary antibodies, followed by incubation with corresponding secondary HRP-conjugated antibodies. The proteins were visualized with an ECL detection reagent (GE HealthCare, Chicago, IL, USA) and a luminescent image analyzer, ImageQuant LAS 4000. The following antibodies were used: anti-NLRP3 (AG-20B-0014, AdipoGen, San Diego, CA, USA), anti-gelsolin (12953, CST, Danvers, MA, USA), anti-ASC (AG-25B-0006, AdipoGen, San Diego, CA, USA), anti-IL-1 $\beta$  (AF-401-NA, R&D systems), anti-Caspase-1 (AG-20B-0042, AdipoGen, San Diego, CA, USA), anti- $\beta$ -actin (4967, CST, Danvers, MA, USA), anti-GAPDH (sc-25778, Santa Cruz, Dallas, TX, USA), anti-acetylated- $\alpha$ -tubulin (sc-23950, Santa Cruz, Dallas, TX, USA), anti-Flightless-I (sc-21716, Santa Cruz, Dallas, TX, USA), anti-p65 (8242, CST, Danvers, MA, USA), anti-I $\kappa$ B $\alpha$  (ab32518, Abcam, Cambridge, UK), anti-phospho-I $\kappa$ B $\alpha$  (9246, CST, Danvers, MA, USA), anti-GSDMD (ab209845, Abcam, Cambridge, UK), anti-TOMM20 (ab56783, Abcam, Cambridge, UK), anti- $\alpha$ -tubulin (E12-054, EnoGene, New York, NY, USA), anti-Flag (F7425, Sigma, St. Louis, MO, USA), anti-Flag (F1804, Sigma, St. Louis, MO, USA) anti-Myc (C3956, Sigma, St. Louis, MO, USA), anti-HA (11867423001, Roche, Basel, Switzerland), and anti-His (ab9108, Abcam, Cambridge, UK). All primary antibodies were diluted to 1:1000. For protein precipitation from cell culture supernatant, an equal volume of methanol and ¼ volume of chloroform were added to the supernatant, mixed thoroughly by vortexing, and the centrifuged at 13000 rpm for 5 min. The upper aqueous phase was discarded, and an equal volume of methanol was added again to the sample. After centrifugation at 13000 rpm for 5 min, the protein pellet was dried at 55 °C and boiled in 1  $\times$  SDS buffer containing 0.1M DTT. The samples were then subjected to immunoblot analysis as described above.

## H. ELISA

The concentrations of cytokine in cell culture supernatants or peritoneal lavage fluid were measured using ELISA kits for mouse IL-1 $\beta$  (BioLegend, San Diego, CA, USA), mouse

IL-18 (Invitrogen, Waltham, MA, USA), mouse IL-6 (BioLegend, San Diego, CA, USA), and mouse TNF $\alpha$  (BioLegend, San Diego, CA, USA), according to the manufacturer's instructions.

### I. RNA isolation and Quantitative real-time PCR

Total RNA was extracted using TRIzol reagent (Invitrogen, Waltham, MA, USA) and cDNA was synthesized by reverse transcription of 2  $\mu$ g RNA. Quantitative real-time PCR was performed with SYBR Green (Invitrogen, Waltham, MA, USA) and detected by LightCycler480 II (LC480; Roche, Basel, Switzerland) with the following cycling conditions: pre-incubation at 95 °C for 5 min, followed by 45 cycles of amplification at 95 °C for 10 s, 60 °C for 10 s, and 72 °C for 10 s. GAPDH was used as an internal control, and the relative gene expression was calculated by the  $2^{-\Delta\Delta C_p}$  method. Specific primer sequences used for qRT-PCR are as follows: *Gapdh*: Forward, 5'-AATCCCATCACCATCTTCCA-3', *Gapdh*: Reverse, 5'-TGGACTCCACGACGTACTCA-3', *Nlrp3*: Forward, 5'-GCCTACAGTTGGGTGAAATGT-3', *Nlrp3*: Reverse, 5'-GGAGGGCTTGATAGCAGTGA-3', *Casp1*: Forward, 5'-TCCGCGGTTGAATCCTTTT CAGA-3', *Casp1*: Reverse, 5'-ACCACAATTGCT GTGTGTGCGCA-3', *Il1b*: Forward, 5'-TCAACCAACAAGTGATATTCTC-3', *Il1b*: Reverse, 5'-ACACAGGACAGGTATAGATTC-3', *Tnf*: Forward, 5'-ATGTCCATTCCTGAGTTCTG -3', *Tnf*: Reverse, 5'-AATCTGGAAAGGTCTGAAGG-3', *HSS-9 eRNA* : Forward, 5'-CATACCCCTCAAAGGACTCTCA-3', and *HSS-9 eRNA* : Reverse, 5'-GGGTCAGTAGCTGGATAACACC-3'.

### J. Cytotoxicity assay

To determine the release of lactate dehydrogenase (LDH) into the culture medium after NLRP3 inflammasome activation, the LDH cytotoxicity assay kit (DoGenBio, Seoul, Korea) was used according to the manufacturer's instructions. For real-time cell death analysis, LPS-primed cells were seeded in a 96-well plate at a density of  $0.5 \times 10^5$  cells/well. After being stimulated with 5  $\mu$ M nigericin and stained with CytotoxGreen, cells were

imaged every 20 min for 3 h by IncuCyte Live-Cell analysis System (Sartorius, Göttingen, Germany).

#### **K. ASC oligomerization assay**

For the ASC oligomerization assay, cells were lysed with PBS containing 0.5% Triton X-100 and a protease inhibitor cocktail (Bio-rad, Hercules, CA, USA), and then centrifuged at 6000 g for 15 min. The Triton X-100 soluble supernatant was collected, while the Triton X-100 insoluble pellet was washed twice with PBS and cross-linked in PBS containing 2 mM disuccinimidyl suberate (Thermo Fisher Scientific, Waltham, MA, USA) and a protease inhibitor cocktail (Bio-rad, Hercules, CA, USA) at 37 °C for 30 min. The cross-linked pellet was dissolved in 1 × SDS buffer and boiled. The Triton X-100 soluble and insoluble fraction samples were subjected to immunoblot analysis.

#### **L. Reconstitution of NLRP3 inflammasome system in HEK293T cells**

HEK293T cells were plated in a 6-well plate at a density of  $1.8 \times 10^6$  cells/well and transfected with plasmids expressing Myc-GSN (500 ng), HA-ASC (350 ng), Flag-NLRP3 (350 ng), and Pro-caspase-1-V5 (1  $\mu$ g) using Lipofectamine 2000 (Invitrogen, Waltham, MA, USA). After 48 h, the indicated cells were stimulated with nigericin (20  $\mu$ M, 45 min), and cleavage of pro-caspase-1 was assessed by immunoblot analysis.

#### **M. Subcellular Fractionation**

The cytosolic and mitochondrial fractions were obtained using a Mitochondria Isolation Kit for Cultured Cells (Thermo Fisher Scientific, Waltham, MA, USA) following the manufacturer's protocol. Each fraction was analyzed by immunoblot analysis and verified by using TOMM20 and  $\alpha$ -tubulin antibodies, respectively.

#### **N. Measurement of intracellular calcium**

For intracellular calcium analysis using microplate reader, LPS-primed peritoneal macrophages were plated in a 96-well black plate with a clear bottom at a density of  $1 \times$

$10^5$  cells/well and stained with 1  $\mu$ M Fluo-4 AM (Invitrogen, Waltham, MA, USA) for 30 min. The cells were then stimulated with 20  $\mu$ M nigericin, 1 mM  $\text{CaCl}_2$ , and 5  $\mu$ M ionomycin at the indicated time. The fluorescence was read for 30 min at 15 s intervals by FLUOstar Omega at 485 nm excitation and 520 nm emission. For intracellular calcium analysis by confocal microscopy, LPS-primed peritoneal macrophages were plated in 8-well Chambered Coverglass (Thermo Fisher Scientific, Waltham, MA, USA) at a density of  $1 \times 10^6$  cells/well and stained with 5  $\mu$ M Fluo-4 AM (Invitrogen, Waltham, MA, USA) for 30 min. Images of untreated cells were acquired ( $t = 0$ ). Then, the cells were stimulated with 20  $\mu$ M nigericin or 1 mM  $\text{CaCl}_2$  and imaged for 30 min with 15 s intervals. At 30 min, 5  $\mu$ M ionomycin was added to the cells, and the cells were further imaged for 10 min at 15 s intervals. Fluorescence images were obtained by Zeiss LSM 980 using 488 nm laser and emission at 525 nm. Images were analyzed by Imaris software.

#### **O. Mitochondrial function assays**

To measure mitochondrial damage, cells were co-stained with 200 nM MitoTracker Green (Invitrogen, Waltham, MA, USA) and 200 nM MitoTracker Deep Red (Invitrogen, Waltham, MA, USA) for 30 min. After washing twice with PBS, cells were resuspended in PBS and subjected to flow cytometry analysis using LSRFortessa X-20 (BD, Franklin Lakes, NJ, USA). To measure mitochondrial ROS production, cells were stained with 5  $\mu$ M MitoSOX Red (Invitrogen, Waltham, MA, USA) for 15 min. After washing twice with PBS, cells were resuspended in PBS and subjected to flow cytometry analysis using LSRFortessa X-20 (BD, Franklin Lakes, NJ, USA).

#### **P. Transmission electron microscopy**

Specimens were fixed in a solution containing 2% glutaraldehyde and 2% paraformaldehyde in 0.1 M phosphate buffer (pH 7.4) for 12 h. They were then washed in 0.1 M phosphate buffer, post-fixed with 1%  $\text{OsO}_4$  in 0.1 M phosphate buffer for 2 h, and dehydrated with an ascending series of ethanol (50%, 60%, 70%, 80%, 90%, 95%, 100%,

100%) for 10 min each. Afterward, specimens were infiltrated with propylene oxide for 10 min, embedded with a Poly/Bed 812 kit (Polysciences, Warrington, PA), and polymerized in an electron microscope oven (TD-700, Dosaka, Kyoto, Japan) at 65 °C for 12 h. The resulting block was equipped with a diamond knife in the ultra-microtome, cut into 200 nm semi-thin sections, and stained with toluidine blue for observation under an optical microscope. The region of interest was then cut into 80 nm thin sections using the ultra-microtome, placed on copper grids, double-stained with 5% uranyl acetate for 20 min and 3% lead citrate for 7 min, and imaged using a transmission electron microscopy (HT7800, Hitachi, Tokyo, Japan) at an acceleration voltage of 80 kV equipped with an RC10 CMOS camera.

#### **Q. Flow cytometry**

PECs were stained with surface markers PerCP-Cyanine5.5-anti-CD11b (Invitrogen, Waltham, MA, USA), FITC-anti-Ly6C (BD, Franklin Lakes, NJ, USA), APC-anti-Ly6G (Invitrogen, Waltham, MA, USA), PE-Cyanine7-anti-F4/80 (Invitrogen, Waltham, MA, USA). Cells were then subjected to flow cytometry analysis using LSRFortessa X-20 (BD, Franklin Lakes, NJ, USA). Data were analyzed by FlowJo software.

#### **R. Immunofluorescence cell staining**

Cells were seeded on coverslips and stimulated with 500 ng/mL LPS for 3 h. For another experiment, LPS-primed macrophages were stimulated with nigericin (5  $\mu$ M) for 45 min. Cells were then fixed and permeabilized with 4% paraformaldehyde and BD Perm/Wash buffer (BD, Franklin Lakes, NJ, USA). Further, cells were incubated overnight at 4 °C with the following primary antibodies: anti-NLRP3 (AG-20B-0014, AdipoGen, San Diego, CA, USA) and anti-ASC (AG-25B-0006, AdipoGen, San Diego, CA, USA), followed by the secondary antibodies: Anti-Mouse IgG –TRITC antibody (T5393, Sigma, St. Louis, MO, USA), and Anti-Rabbit IgG –FITC antibody (F9887, Sigma, St. Louis, MO, USA) for 1 h at RT. Mitochondria were labeled with MitoTracker Deep Red (Invitrogen, Waltham, MA,

USA) and nuclei were counterstained with DAPI. Confocal images were acquired using a Zeiss LSM 980 laser scanning microscope (Carl Zeiss, Jena, Germany).

### **S. MSU-induced peritonitis**

Male mice aged 6–10 weeks were intraperitoneally injected with 1 mg MSU crystals dissolved in sterile PBS or the same volume of sterile PBS (control). After 6 h, the peritoneal cavities were washed with 10 mL of sterile PBS, and the peritoneal lavage fluid was collected. The supernatant was concentrated by Amicon ultra centrifugal filter to measure cytokine level with ELISA. PECs were analyzed by FACS to determine immune cell infiltration.

### **T. LPS-induced septic shock**

Male mice aged 6–10 weeks were intraperitoneally injected with 20 mg/kg LPS (*Escherichia coli* O111:B4, Sigma, St. Louis, MO, USA) or the same volume of sterile PBS as a control. After 3 h, serum and peritoneal lavage fluid were collected. The peritoneal lavage fluid was concentrated using an Amicon ultra centrifugal filter, and both serum and peritoneal lavage fluid samples were analyzed by ELISA. For the survival test, mice were intraperitoneally injected with 10 mg/kg of LPS (*Escherichia coli* O111:B4, Sigma, St. Louis, MO, USA) or PBS as a control. The mice were then monitored every 6 h for 96 h.

## **2. Assays for cancer research**

### **A. Cell culture and transfection**

The human HCC cell line FT3-7 cells were cultured in DMEM (Hyclone, Logan, UT, USA) supplemented with 10% fetal bovine serum (FBS; Hyclone, Logan, UT, USA), Penicillin-Streptomycin (Gibco, Waltham, MA, USA) in an incubator containing 5% CO<sub>2</sub> at 37 °C. Cells were treated with 5-fluorouracil (5-FU) (Sigma, St. Louis, MO, USA) at indicated doses and time. ASOs used to knockdown *THUMPD3-AS1*, *LINC01572*, and *PLEKHA8P1* gene were designed and purchased alongside negative control ASOs from Qiagen.  $5 \times 10^5$

cells were seeded in 6-well plates and ASOs (20 nM) were transfected into cells with Lipofectamine RNAiMax (Invitrogen, Waltham, MA, USA) as per manufacturer's instructions. A second transfection was conducted after 24 h to increase knockdown efficiency. The ASO sequences are as follows: Negative control ASO: 5'-AACACGTCTATACGC-3', *THUMPD3-AS1* ASO: 5'-GACACCTTAGAAAATT-3', *LINC01572* ASO: 5'-ACATAGAGACAGACTG-3', *PLEKHA8P1* ASO 1: 5'-TTGCTGTGAAATCATG-3', and *PLEKHA8P1* ASO 2: 5'-ACACTTTAGCACTTTA-3'.

### **B. RNA isolation and quantitative real-time PCR**

Total RNA was extracted from cultured cells with TRIzol reagent (Invitrogen, Waltham, MA, USA) and reverse transcriptase PCR (RT-PCR) was conducted with 2 µg of RNA. qRT-PCR was carried out using SYBR Green dye (Invitrogen, Waltham, MA, USA) and detected by LightCycler480 II (LC480; Roche, Basel, Switzerland) with the following cycling conditions: pre-incubation at 95 °C for 5 min, followed by 45 cycles of amplification at 95 °C for 10 s, 60 °C for 10 s, and 72 °C for 10 s. The relative gene expression levels were normalized to GAPDH and calculated by the  $2^{-\Delta\Delta C_p}$  method. The primer sequences used for qRT-PCR are as follows: *GAPDH*: Forward, 5'-AATCCCATCACCATCTTCCA-3', *GAPDH*: Reverse, 5'-TGGACTCCACGACGTACTCA-3', *PLEKHA8P1*: Forward, 5'-CAGCCTTTACCTCCCTGCCA-3', and *PLEKHA8P1*: Reverse, 5'-TGCCCAGCAGCCATCATACA-3'.

### **C. Cell counting kit-8 assay**

Cell proliferation was assessed by cell counting kit-8 (CCK-8; Dojindo, Kumamoto, Japan) assays following the manufacturer's protocol. In brief, cells were seeded in 96-well plates, and 10 µl of CCK-8 reagent was added at the indicated time points (0, 24, 48, and 72 h). Cell viability was measured with a microplate reader (Molecular Devices, San Jose, CA, USA) at 450 nm.

#### **D. IncuCyte® cell proliferation assay**

The cells were plated in 96-well plates (3595, Corning Inc., Corning, NY, USA). The proliferation of cells was monitored for 4 days by an IncuCyte Live-Cell analysis system (Sartorius, Göttingen, Germany).

#### **E. Colony formation assay**

Following transfection,  $2 \times 10^3$  cells were seeded in 6-well plates and cultured for 12 days. Cells were fixed using 4% paraformaldehyde and stained with 1% crystal violet for colony enumeration.

#### **F. Invasion and migration assays**

24-well transwell plates (8  $\mu$ m pore size, 3422, Corning Inc., Corning, NY, USA) were used for invasion and migration assays. For invasion assays, transwell inserts were coated with Matrigel (354234, Corning Inc., Corning, NY, USA) diluted in serum-free medium. A total of  $3 \times 10^4$  cells resuspended in serum-free medium were seeded in the inserts, while 600  $\mu$ L of medium containing 10% FBS was added into the lower chamber. After 24–48 h, invaded cells were fixed with 4% paraformaldehyde and stained with 1% crystal violet. For migration assays, the lower side of the insert was coated with gelatin (G1393, Sigma, St. Louis, MO, USA) diluted in PBS. A total of  $1.5 \times 10^4$  cells resuspended in serum-free medium were seeded in inserts while 600  $\mu$ L of medium containing 10% FBS was added to the lower chamber. Following 24–48 h, migrated cells were fixed with 4% paraformaldehyde and stained with 1% crystal violet. Six random fields per well were photographed by microscopy (Carl Zeiss, Jena, Germany) and counted.

#### **G. Wound-healing assay**

Transfected cells were seeded in 96-well ImageLock plate (4379, Sartorius, Göttingen, Germany) at a density of  $3 \times 10^4$  cells/well. Wounds were created by IncuCyte WoundMaker Tool (4563, Sartorius, Göttingen, Germany) and cell debris were removed

by washing with  $1 \times$  PBS. Cells were monitored and analyzed by IncuCyte Live-Cell analysis System (Sartorius, Göttingen, Germany) for up to 3 days.

### III. RESULTS

#### 1. Regulation of IL-1 $\beta$ expression: Gelsolin-mediated negative modulation of NLRP3 inflammasome activation

##### A. Gelsolin binds to NLRP3 at the priming step

According to a study conducted by a co-worker, it has been revealed through IP-MS that gelsolin binds to NLRP3 in LPS-primed BMDMs prior to assembly and activation of the NLRP3 inflammasome complex. Upon stimulation, NLRP3 oligomerizes itself and recruits ASC to form an inflammasome complex with caspase-1<sup>3</sup>. Following nigericin stimulation, NLRP3 was shifted to the high molecular mass fraction, forming an NLRP3 inflammasome complex, as shown by gel filtration chromatography (Figure 1A). In LPS-primed BMDMs, gelsolin was found to co-exist with NLRP3 already, while ASC and pro-caspase-1 were co-eluted with NLRP3 after stimulation with nigericin (Figure 1A). These results suggest that gelsolin forms a complex with NLRP3 before ASC recruitment. To identify whether gelsolin directly binds to NLRP3, I transiently co-transfected NLRP3 and gelsolin into HEK293T cells. Co-immunoprecipitation (Co-IP) assay revealed that gelsolin was co-eluted with NLRP3 when using anti-Flag antibody, and vice versa (Figures 1B and 1C). Together, these results indicate that gelsolin interacts with NLRP3 during the priming stage before inflammasome assembly.

I then tried to determine whether gelsolin is directly associated with other NLRP3 inflammasome components. I transiently co-expressed gelsolin with ASC, pro-caspase-1, or NEK7, a recently identified as an inflammasome component<sup>47,48</sup>. I confirmed that gelsolin does not bind directly to other inflammasome components except NLRP3 (Figures 1D-1F).

I then investigated which regions of NLRP3 and gelsolin are required for their interaction. To do this, I constructed various truncated mutants of these two proteins and found that NLRP3<sup>LRR</sup> has a defect in binding to gelsolin (Figure 1G) and GSN<sup>C</sup> has a defect

in binding to NLRP3 (Figure 1H), suggesting that NACHT and PYD of NLRP3 and N-terminus of gelsolin are indispensable for their interaction.

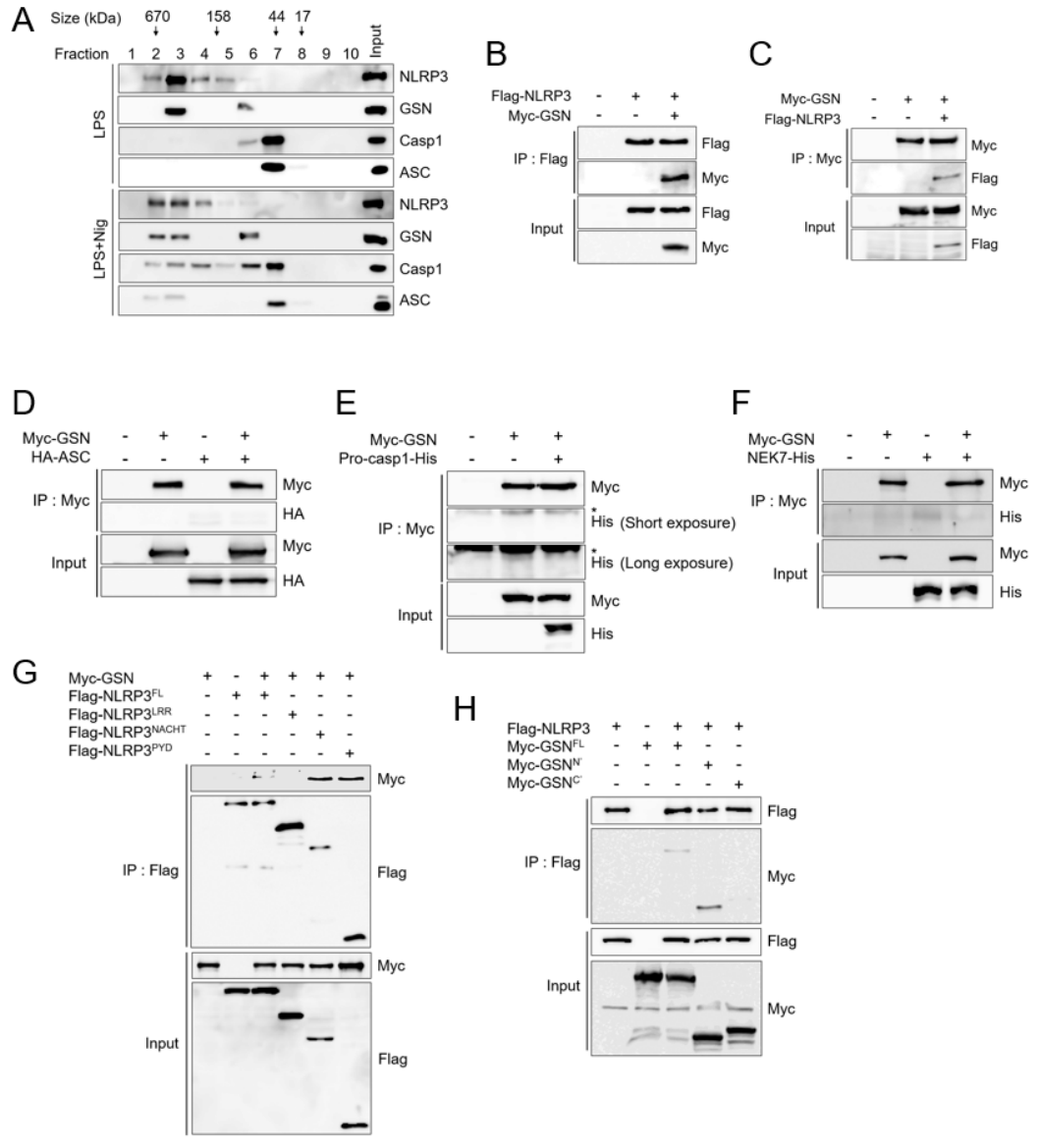


**Figure 1. Gelsolin interacts with NLRP3 in LPS-primed macrophages.** (A) Immunoblots of cell lysate in murine BMDMs primed with LPS (500 ng/mL, 3 h), and primed and stimulated with nigericin (5 μM, 45 min), and then fractionated using gel-

filtration chromatography. (B-H) Immunoblots of co-immunoprecipitated proteins with anti-Flag antibody (B, G, H) or anti-Myc antibody (C-F) in HEK293T cells transiently transfected with Flag-NLRP3, Myc-GSN, HA-ASC, pro-Caspase-1-His, NEK7-His, Flag-NLRP3<sup>LRR</sup>, Flag-NLRP3<sup>NACHT</sup>, Flag-NLRP3<sup>PYD</sup>, Myc-GSN<sup>N</sup>, and Myc-GSN<sup>C</sup>. Asterisks (\*) indicate a heavy chain (50 kDa). Data shown in B-H are representative of at least three independent experiments.

## **B. Gelsolin negatively regulates NLRP3 inflammasome activation and pyroptosis**

To elucidate the biological function of gelsolin in the NLRP3 inflammasome activation pathway, a co-worker generated gelsolin-deficient J774.1 cell clone and myeloid cell-specific gelsolin deleted mice. To determine whether gelsolin affects the NLRP3 inflammasome pathway, I first examined the cleavage of pro-IL-1 $\beta$  and pro-caspase-1 induced by nigericin. *Gsn*<sup>ΔMye</sup> BMDMs showed excessive secretion of matured IL-1 $\beta$  (p17) and caspase-1 (p20) into the supernatant compared to *Gsn*<sup>fl/fl</sup> BMDMs (Figures 2A and 2B). In addition, the levels of secreted IL-18, which is also released when the NLRP3 inflammasome is activated<sup>6</sup>, were found to be elevated in *Gsn*<sup>ΔMye</sup> BMDMs compared to *Gsn*<sup>fl/fl</sup> BMDMs (Figure 2C), while there was no effect observed on the release of TNF $\alpha$  (Figure 2D). Upon activation, ASC undergoes oligomerization through homotypic PYD-PYD interaction<sup>6</sup>. I observed that the oligomerization of ASC is increased in *Gsn*<sup>ΔMye</sup> BMDMs compared to *Gsn*<sup>fl/fl</sup> BMDMs (Figures 2E and 2F). Moreover, the results from gel filtration chromatography were in agreement with these findings, revealing an increased co-elution of ASC and caspase-1 with NLRP3 that had shifted into a high molecular weight fraction in *Gsn*<sup>ΔMye</sup> BMDMs when compared to WT BMDMs (Figures 2G and 1A). The assembly of ASC into oligomers can be observed as a microscopic 'speck,' and I noticed a notable rise in the number of ASC specks in *Gsn*<sup>ΔMye</sup> BMDMs in comparison to those in *Gsn*<sup>fl/fl</sup> BMDMs (Figure 2H). This suggests that the absence of gelsolin promotes the formation of the NLRP3 inflammasome. Similar results were obtained in nigericin-stimulated *Gsn*-KO J774.1 cells (Figures 2I–2N). NLRP3 inflammasome activators induce the accumulation of acetylated- $\alpha$ -tubulin, which mediates microtubule-dependent inflammasome activation<sup>51</sup>. I observed that there was no significant difference in the accumulation of acetylated- $\alpha$ -tubulin between control and *Gsn*-KO J774.1 cells (Figure 2I). To further clarify the inhibitory effect of gelsolin on NLRP3 inflammasome activation, I utilized the NLRP3 inflammasome reconstitution system in HEK293T cells. Reconstitution of NLRP3 inflammasome by overexpressing NLRP3, ASC, and pro-caspase-1 in

HEK293T cells lacking endogenous inflammasome proteins is sufficient to trigger the maturation of pro-caspase-1 upon nigericin stimulation<sup>49,50</sup>. As expected, overexpression of gelsolin inhibited the cleavage of caspase-1 induced by nigericin (Figure 2O). Additionally, gelsolin is also not involved in LPS-induced NF- $\kappa$ B activation, as evidenced by the comparable level of NF- $\kappa$ B activation and mRNA expression of *Nlrp3*, *Casp1*, and *Il1b* in *Gsn*<sup>ΔMye</sup> and *Gsn*<sup>fl/fl</sup> BMDMs (Figures 3A-3E).

Furthermore, my results indicate that the absence of gelsolin leads to an increase in NLRP3 inflammasome-dependent pyroptotic cell death, which can be determined by the generation of GSDMD N-terminal fragment (GSDMD-N) and the release of lactate dehydrogenase (LDH) (Figures 4A and 4B). Live cell imaging also shows that more dead cells were stained with CytotoxGreen in the absence of gelsolin (Figures 4C and 4D). Similar results were obtained *Gsn*-KO J774.1 cell lines (Figures 4E and 4F). Collectively, my results demonstrate that gelsolin specifically inhibits NLRP3 inflammasome activation and caspase-1-mediated pyroptosis.

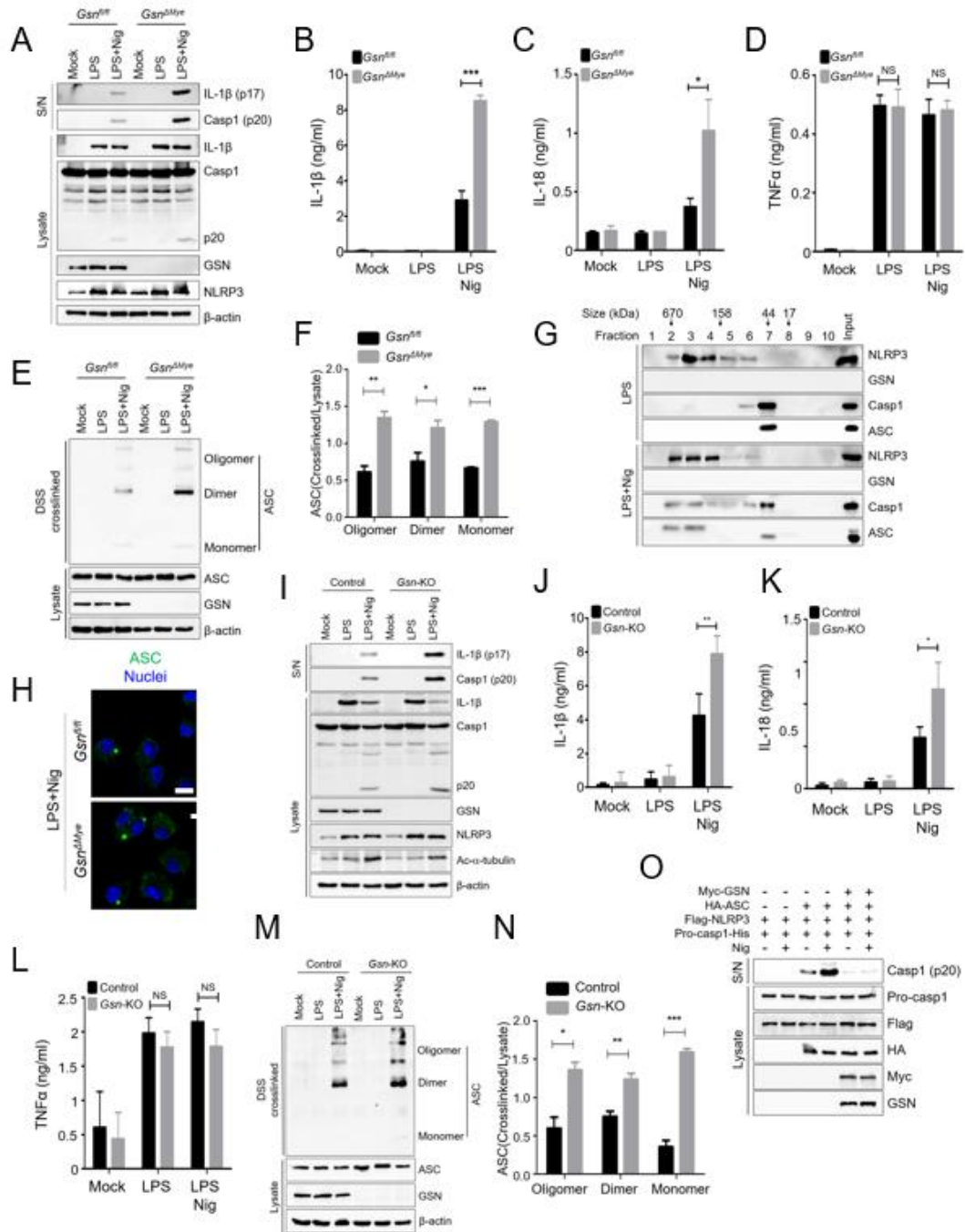


**Figure 2. Gelsolin deficiency results in excessive NLRP3 inflammasome activation.** (A) Immunoblots of supernatant (S/N) and cell lysates (Lysate) in *Gsn<sup>fl/fl</sup>* and *Gsn<sup>ΔMye</sup>* BMDMs left untreated, primed with LPS (500 ng/mL, 3 h), and primed and stimulated with nigericin (5 μM, 45 min). (B-D) ELISA for IL-1β (B), IL-18 (C), and TNFα (D) in the supernatant of *Gsn<sup>fl/fl</sup>* and *Gsn<sup>ΔMye</sup>* BMDMs left untreated, primed with LPS (500 ng/mL, 3 h), and primed and stimulated with nigericin (5 μM, 45 min) (n = 3). NS, not significant. (E, F) ASC oligomerization of DSS cross-linked pellets in *Gsn<sup>fl/fl</sup>* and *Gsn<sup>ΔMye</sup>* BMDMs left untreated, primed with LPS (500 ng/mL, 3 h), and primed and stimulated with nigericin (5 μM, 45 min). The intensity of immunoblot bands were quantified using imageJ software (F) (n = 3). (G) Immunoblots of cell lysate in *Gsn<sup>ΔMye</sup>* BMDMs primed with LPS (500 ng/mL, 3 h), and primed and stimulated with nigericin (5 μM, 45 min), and then fractionated using gel-filtration chromatography. (H) Immunofluorescence staining of ASC in *Gsn<sup>fl/fl</sup>* and *Gsn<sup>ΔMye</sup>* BMDMs primed with LPS (500 ng/mL, 3 h) and stimulated with nigericin (5 μM, 45 min). ASC, green; nuclei, blue. Scale bar, 10 μm. (I) Immunoblots of supernatant (S/N) and cell lysates (Lysate) in control and *Gsn*-KO J774.1 cells left untreated, primed with LPS (500 ng/mL, 3 h), and primed and stimulated with nigericin (5 μM, 45 min). (J-L) ELISA for IL-1β (J), IL-18 (K), and TNFα (L) in the supernatant of control and *Gsn*-KO J774.1 cells left untreated, primed with LPS (500 ng/mL, 3 h), and primed and stimulated with nigericin (5 μM, 45 min) (n = 4). NS, not significant. (M, N) ASC oligomerization of DSS cross-linked pellets in control and *Gsn*-KO J774.1 cells left untreated, primed with LPS (500 ng/mL, 3 h), and primed and stimulated with nigericin (5 μM, 45 min). The intensity of immunoblot bands were quantified using imageJ software (N) (n = 3). (O) Immunoblots of supernatant (S/N) and cell lysates (Lysate) in HEK293T cells transiently transfected with Myc-GSN, HA-ASC, Flag-NLRP3, and pro-Caspase-1-His stimulated with nigericin (20 μM, 45 min). Data are presented as means ± SD (B-D, J-L) or means ± SEM (F, N). Student's t-test, \**p* < 0.05, \*\**p* < 0.01, \*\*\**p* < 0.001 (B, C, F, J, K, N). Data shown in A, E, I, M, O are representative of at least three independent experiments.

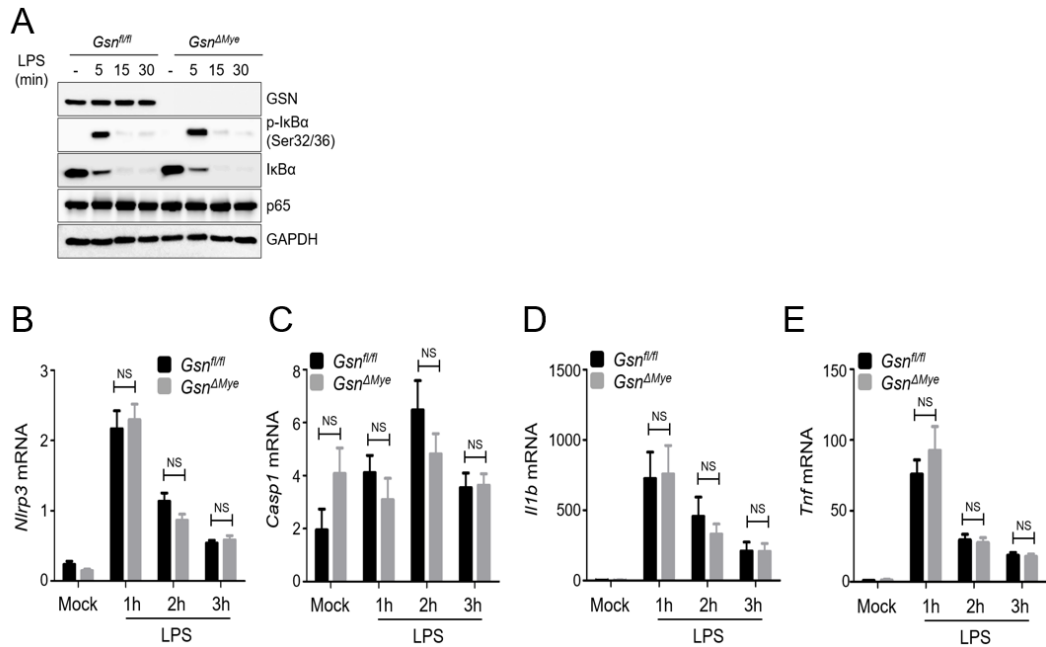


**Figure 3. Gelsolin does not affect the NF- $\kappa$ B pathway.** (A) Immunoblots for I $\kappa$ B $\alpha$ , the phosphorylated form of the serine 32 and 36 region of I $\kappa$ B $\alpha$ , and p65 in *Gsn<sup>fl/fl</sup>* and *Gsn<sup>ΔMyc</sup>* BMDMs left untreated or primed with LPS (500 ng/mL) for the indicated time. (B-E) qRT-PCR analysis for mRNA expression of NLRP3 (B), pro-Caspase-1 (C), pro-IL-1 $\beta$  (D), and TNF $\alpha$  (E). mRNA expression of each gene was normalized to the internal control GAPDH (n = 19). NS, not significant (Student's t-test). Data are presented as means  $\pm$  SEM (B-E). Data shown in A are representative of at least three independent experiments.

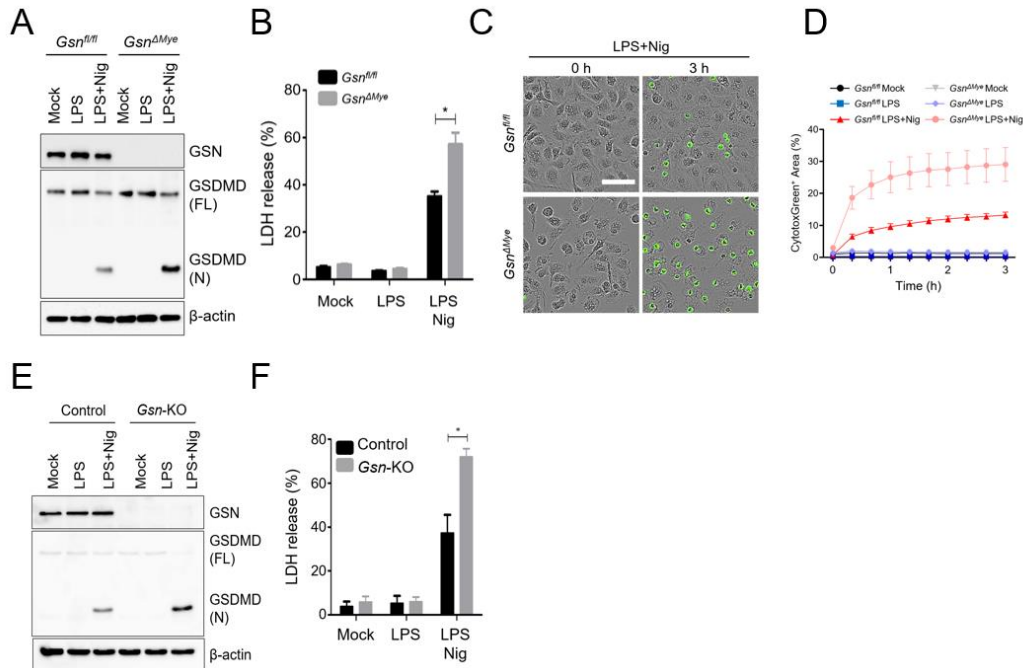


**Figure 4. Gelsolin deficiency promotes pyroptotic cell death.** (A) Immunoblots for full length and cleaved GSDMD of *Gsn<sup>fl/fl</sup>* and *Gsn<sup>ΔMye</sup>* BMDMs left untreated, primed with LPS (500 ng/mL, 3 h), and primed and stimulated with nigericin (5 μM, 45 min). (B) LDH release into the supernatant of *Gsn<sup>fl/fl</sup>* and *Gsn<sup>ΔMye</sup>* BMDMs left untreated, primed with LPS (500 ng/mL, 3 h), and primed and stimulated with nigericin (5 μM, 45 min) (n = 3). (C, D) Representative IncuCyte images (C) and quantification (D) of CytotoxGreen-positive dead cells in *Gsn<sup>fl/fl</sup>* and *Gsn<sup>ΔMye</sup>* BMDMs left untreated, primed with LPS (500 ng/mL, 3 h), and primed and stimulated with nigericin (5 μM, 45 min). Scale bar, 50 μm (n = 6). (E) Immunoblots for full length and cleaved GSDMD of control and *Gsn-KO* J774.1 cells left untreated, primed with LPS (500 ng/mL, 3 h), and primed and stimulated with nigericin (5 μM, 45 min). (F) LDH release into the supernatant of control and *Gsn-KO* J774.1 cells left untreated, primed with LPS (500 ng/mL, 3 h), and primed and stimulated with nigericin

(5  $\mu$ M, 45 min) (n = 3). Data are presented as means  $\pm$  SEM (B, D, F). Student's t-test, \* $p$  < 0.05 (B, F). Data shown in A, E are representative of at least three independent experiments.

### **C. Gelsolin inhibits the translocation of NLRP3 to mitochondria during the priming process by disturbing the association between NLRP3 and a mitochondrial protein MAVS**

Under resting conditions, NLRP3 is located on the endoplasmic reticulum (ER), while it associates with ASC on the mitochondria at the perinuclear region in a microtubule-dependent manner after stimulation<sup>51,52</sup>. Studies have suggested that upon stimulation, NLRP3 associates with the mitochondria-associated ER membranes (MAMs)<sup>10</sup> or golgi apparatus<sup>49,53</sup>, particularly with dispersed trans-golgi network (dTGN)<sup>54</sup>. Ultimately, the NLRP3 inflammasome is assembled and activated at the microtubule organizing center (MTOC)<sup>55-57</sup>. Although the exact subcellular localization of NLRP3 is still being debated, it is undeniable that mitochondrial translocation of NLRP3 is a crucial initial step for NLRP3 inflammasome activation, given that LPS priming alone is sufficient to induce NLRP3 to associate with the mitochondria<sup>58</sup>.

Since gelsolin interacts with NLRP3 following LPS priming alone, I hypothesized that gelsolin would affect the pathway of NLRP3 translocation to the mitochondria. I isolated cytosolic and mitochondrial fractions respectively, and confirmed that NLRP3 was detected in the mitochondrial fraction during the priming stage. I found that NLRP3 was more translocated to the mitochondria in *Gsn*-KO J774.1 cells compared to control J774.1 cells, implying gelsolin prevents NLRP3 from moving to the mitochondria (Figures 5A-5C). Interestingly, gelsolin was observed to move to the mitochondria upon stimulation with nigericin, presumably as a free gelsolin that does not interact with NLRP3. Similar results were obtained in *Gsn*<sup>*ΔMye*</sup> BMDMs (Figure 5D). These results were additionally supported by immunocytochemistry, which demonstrated that NLRP3 and mitochondria co-localize following LPS priming, and this co-localization is even more pronounced in the absence of gelsolin (Figure 5E).

NLRP3 inflammasome stimuli cause the mitochondrial outer membrane protein MAVS to interact with NLRP3, facilitating NLRP3 translocation to the mitochondria<sup>52</sup>.

Therefore, I conducted Co-IP experiments to investigate whether gelsolin affects the interaction between NLRP3 and MAVS. NLRP3 and MAVS were co-transfected with varying amounts of gelsolin, and it was observed that the interaction between NLRP3 and MAVS gradually decreased as the amount of gelsolin increased, verifying that gelsolin competes with MAVS to interact with NLRP3 (Figures 6A and 6B). However, when NLRP3 and gelsolin were co-transfected with varying amounts of MAVS, the interaction between NLRP3 and gelsolin was unaffected, indicating that the affinity of gelsolin to NLRP3 may be higher than that of MAVS to NLRP3 (Figures 6C and 6D). Taken together, these findings indicate that gelsolin prevents NLRP3 from moving to the mitochondria by interfering the interaction between NLRP3 and MAVS.

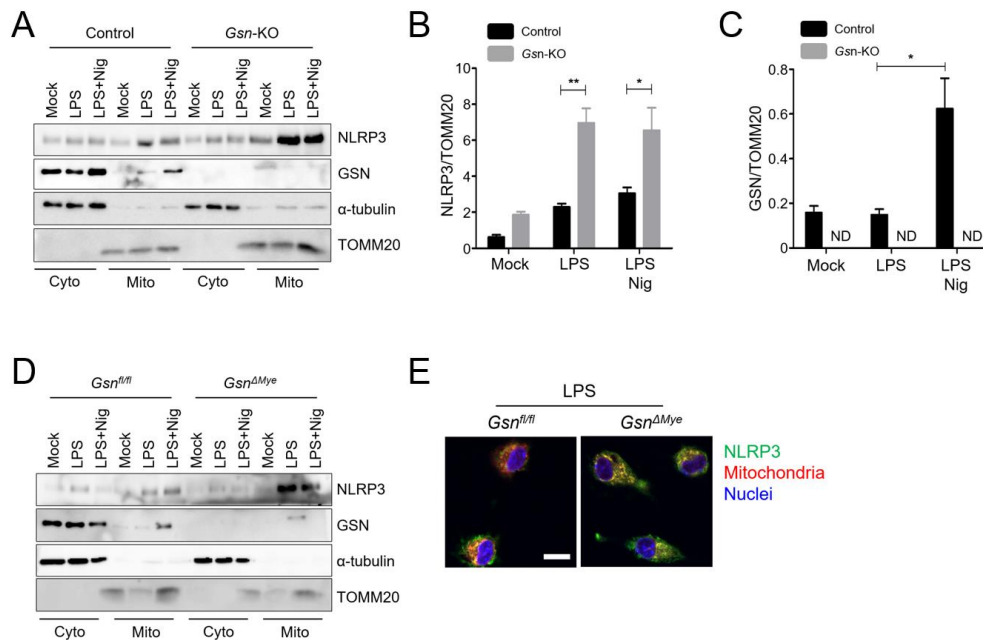


**Figure 5. Gelsolin depletion promotes the translocation of NLRP3 to mitochondria.** (A-C) Immunoblots of the cytosolic and mitochondrial fraction in control and *Gsn*-KO J774.1 cells left untreated, primed with LPS (500 ng/mL, 3 h), and primed and stimulated with nigericin (5  $\mu$ M, 45 min). The intensity of immunoblot bands were quantified using imageJ software (B, C) (n = 4). ND, not detected. (D) Immunoblots of the cytosolic and mitochondrial fraction in *Gsn*<sup>fl/fl</sup> and *Gsn* <sup>$\Delta$ Mye</sup> BMDMs left untreated, primed with LPS (500 ng/mL, 3 h), and primed and stimulated with nigericin (5  $\mu$ M, 45 min). (E) Immunofluorescence staining of NLRP3 and labeling mitochondria/nuclei in *Gsn*<sup>fl/fl</sup> and *Gsn* <sup>$\Delta$ Mye</sup> BMDMs primed with LPS (500 ng/mL, 3 h). NLRP3, green; mitochondria, red; nuclei, blue. Scale bar, 10  $\mu$ m. Data are presented as means  $\pm$  SEM (B, C). Student's t-test, \* $p$  < 0.05, \*\* $p$  < 0.01 (B, C). Data shown in A is representative of at least three independent experiments.

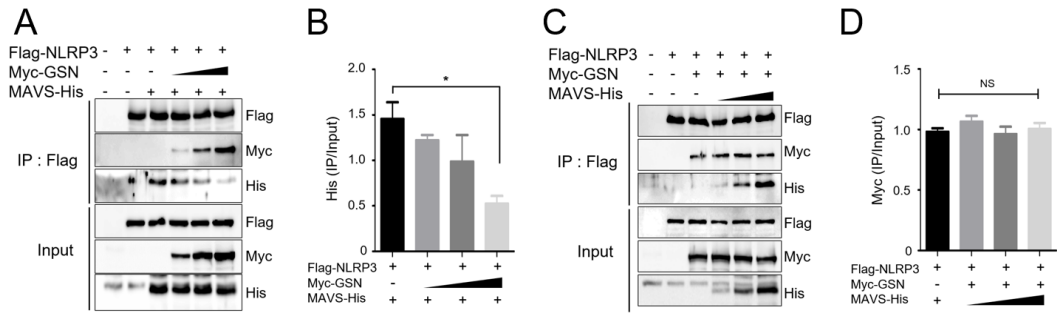


**Figure 6. Gelsolin inhibits the association between NLRP3 and MAVS.** (A-D) Immunoblots of co-immunoprecipitated proteins with anti-Flag antibody in HEK293T cells transiently transfected with Myc-GSN, Flag-NLRP3, and MAVS-His. The intensity of immunoblot bands was quantified using imageJ software (B, D) (n = 3). NS, not significant. Data are presented as means  $\pm$  SEM (B, D). Student's t-test,  $*p < 0.05$  (B, D). Data shown in A and C are representative of at least three independent experiments.

#### **D. Gelsolin serves as a reservoir for calcium and maintains mitochondrial stability**

Gelsolin can be activated by various factors, including the concentration of intracellular calcium<sup>16</sup>. I investigated whether gelsolin activity influences the interaction between NLRP3 and gelsolin. When intracellular calcium was chelated using BAPTA-AM, the interaction between NLRP3 and gelsolin decreased in a dose-dependent manner. This finding demonstrates that calcium-activated gelsolin binds to NLRP3 (Figures 7A and 7B).

Gelsolin, with its multiple calcium binding sites, functions to effectively sequester calcium ions upon binding<sup>16</sup>. I hypothesized that because gelsolin keeps calcium for binding to NLRP3 in normal states, the concentration of free intracellular calcium would be higher in gelsolin-deficient macrophages than in control macrophages. As it is known that NLRP3 inflammasome stimuli promote calcium mobilization<sup>59</sup>, nigericin and CaCl<sub>2</sub> stimulation triggered influx of calcium into the cytosol. My findings indicate that this influx was significantly promoted in *Gsn*<sup>ΔMye</sup> peritoneal macrophages (Figures 8A and 8B). These results were corroborated and visualized microscopically (Figures 8C-8F).

Calcium signaling is associated with NLRP3 inflammasome activation. NLRP3 inflammasome activation is triggered by an increase in cytosolic calcium resulting from extracellular calcium treatment or calcium release from the ER<sup>60</sup>. Elevated intracellular calcium levels can lead to calcium uptake by mitochondria, which can cause calcium overload and mitochondrial destabilization. Damaged mitochondria can produce mROS, which can activate NLRP3 inflammasome<sup>10,61</sup>.

Mitochondrial damage can be assessed by loss of mitochondrial membrane potential ( $\Delta\Psi_m$ )<sup>61</sup>. I found that gelsolin depletion leads to excessive  $\Delta\Psi_m$  loss, determined by decreased respiratory mitochondria (Figures 9A and 9B). Consistent with these results, mROS generation were promoted in *Gsn*<sup>ΔMye</sup> BMDMs compared to *Gsn*<sup>fl/fl</sup> BMDMs (Figures 9C and 9D). Transmission electron microscopy (TEM) allows for the visualization of the internal structure of mitochondria. Mitochondrial structural defects can be identified

by the presence of electron-dense structures<sup>62</sup>. When exposed to nigericin stimulation, the accumulation of electron-dense mitochondria was facilitated, and this effect was greatly exacerbated in the absence of gelsolin, as evidenced by highly disrupted cristae (Figure 9E). Similar findings were acquired in *Gsn*-KO J774.1 cell lines (Figures 9F-9I). These results support the idea that gelsolin serves as a calcium reservoir to bind with NLRP3, preventing NLRP3 inflammasome from being activated by mitochondrial damage.

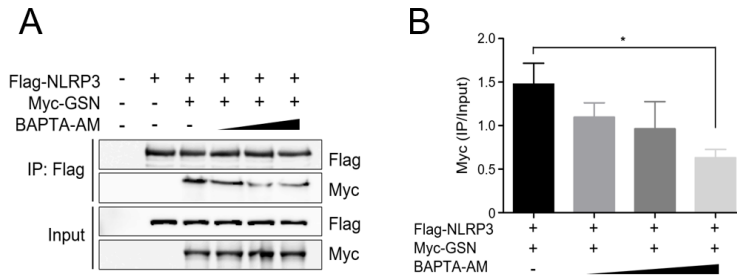


**Figure 7. The association between gelsolin and NLRP3 is dependent on calcium.** (A, B) Immunoblots of co-immunoprecipitated proteins with anti-Flag antibody in HEK293T cells transiently transfected with Myc-GSN and Flag-NLRP3 in the presence (5  $\mu$ M, 20  $\mu$ M, and 40  $\mu$ M) or absence of BAPTA-AM (A). The intensity of immunoblot bands was quantified using imageJ software (B) (n = 3). Data are presented as means  $\pm$  SEM (B). Student's t-test, \* $p$  < 0.05 (B). Data shown in A are representative of at least three independent experiments.

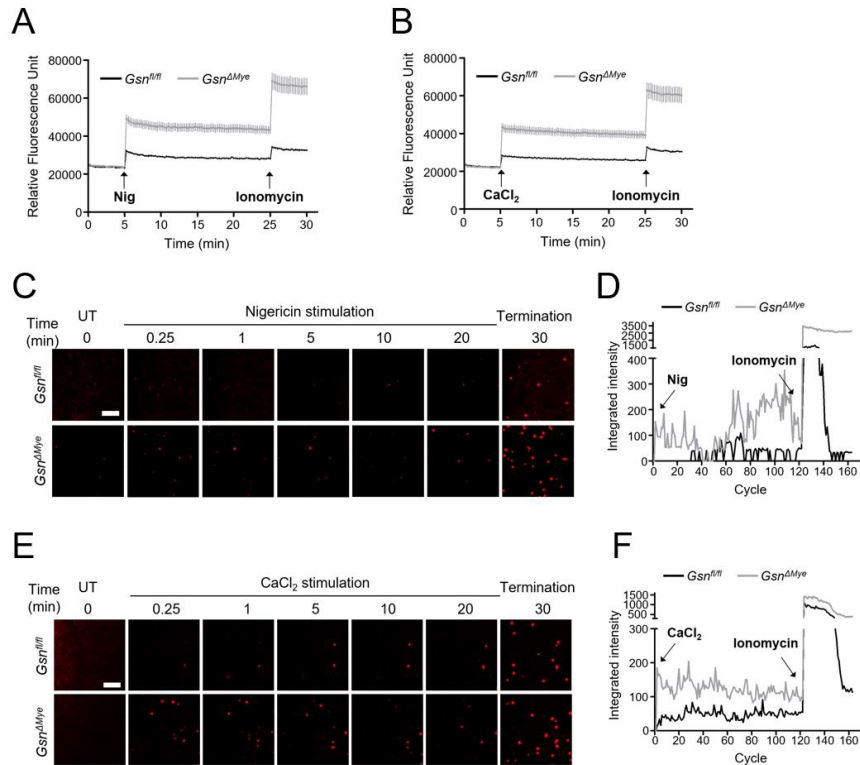


**Figure 8. Intracellular calcium concentration is increased in the absence of gelsolin.** (A, B) Calcium influx was analyzed in LPS-primed peritoneal macrophages in response to nigericin (20  $\mu$ M) (A) or CaCl<sub>2</sub> (1 mM) (B) stimulation using a microplate reader. Ca<sup>2+</sup> ionophore ionomycin (5  $\mu$ M) was added after 25 min (n = 10). (C-F) Representative confocal microscopy images (C, E) and quantification (D, F) of calcium influx in LPS-primed peritoneal macrophages in response to nigericin (20  $\mu$ M) (C, D) or CaCl<sub>2</sub> (1 mM) (E, F) stimulation. Ca<sup>2+</sup> ionophore ionomycin (5  $\mu$ M) was added after 30 min and cells were further imaged for 10 min. Scale bar, 50  $\mu$ m. Data are presented as means  $\pm$  SEM (A, B).

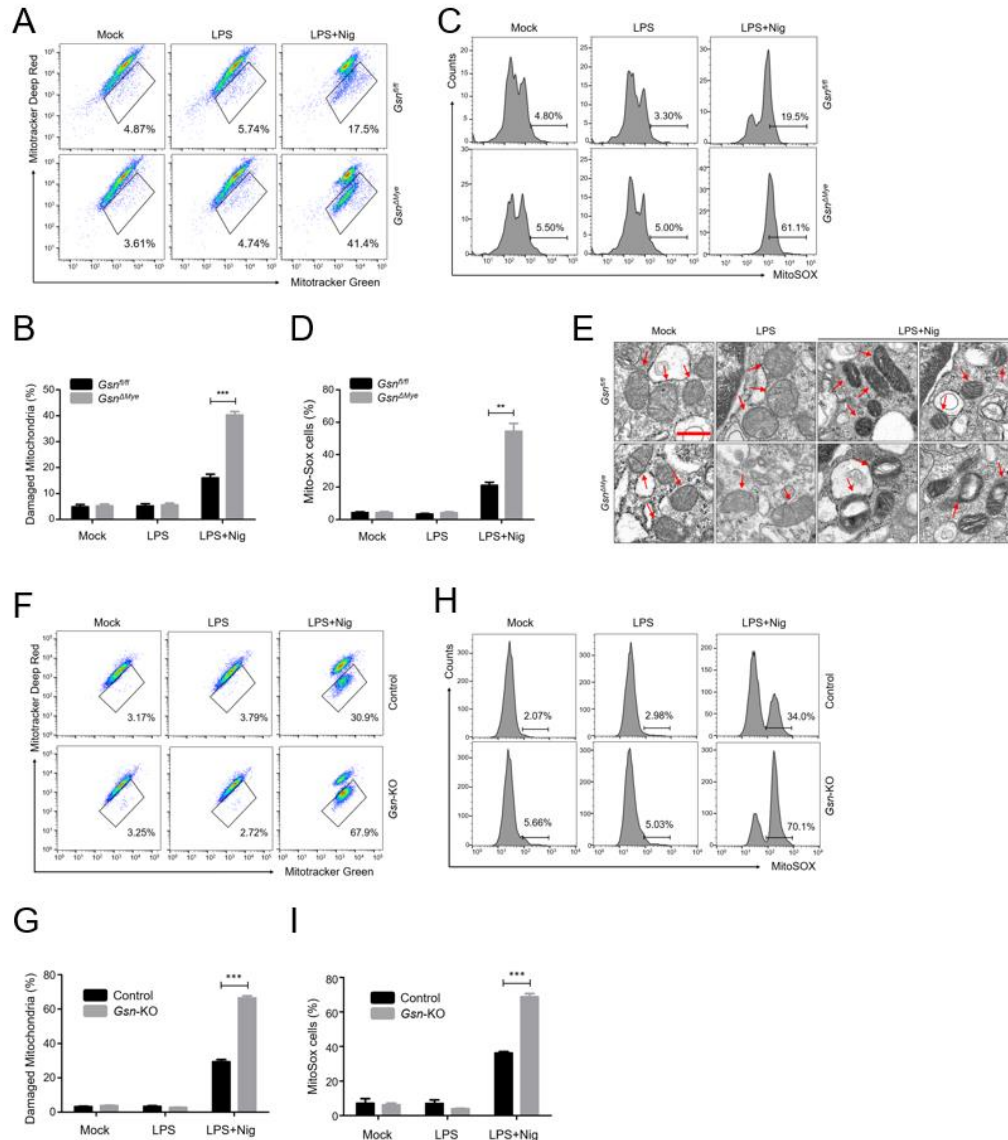


**Figure 9. Ablation of gelsolin promotes mitochondrial dysfunction.** (A-D) Representative images (A, C) and quantification (B, D) of damaged mitochondria (A, B) ( $n = 4$ ) and MitoSOX-positive mitochondria (C, D) ( $n = 3$ ) in *Gsn<sup>fl/fl</sup>* and *Gsn<sup>ΔMye</sup>* BMDMs

left untreated, primed with LPS (500 ng/mL, 3 h), and primed and stimulated with nigericin (10  $\mu$ M, 1 h) (A, B), nigericin (20  $\mu$ M, 45 min) (C, D) determined by flow cytometry. (E) Representative TEM images of mitochondria in *Gsn<sup>f/f</sup>* and *Gsn<sup>AMye</sup>* peritoneal macrophages left untreated, primed with LPS (500 ng/mL, 3 h), and primed and stimulated with nigericin (5  $\mu$ M, 45 min). To avoid bias, at least 10 images per sample were acquired. Red arrows indicate mitochondria. Scale bar, 5  $\mu$ m. (F-I) Representative images (F, H) and quantification (G, I) of damaged mitochondria (F, G) (n = 4) and MitoSOX-positive mitochondria (H, I) (n = 4) in control and *Gsn*-KO J774.1 cells left untreated, primed with LPS (500 ng/mL, 3 h), and primed and stimulated with nigericin (5  $\mu$ M, 45 min) determined by flow cytometry. Data are presented as means  $\pm$  SEM (B, D, G, I). Student's t-test, \*\* $p$  < 0.01, \*\*\* $p$  < 0.001 (B, D, G, I). Data shown in A, C, F, H are representative of at least two independent experiments.

### **E. Gelsolin inhibits NLRP3 inflammasome activation *in vivo***

To further investigate the protective function of gelsolin in a physiological environment, I utilized two mouse models related to NLRP3 inflammasome. MSU crystals, which derive gout, induce neutrophil infiltration and IL-1 $\beta$  secretion in an NLRP3 inflammasome-dependent manner when directly injected into the peritoneum<sup>63,64</sup>. As expected, intraperitoneal administration of MSU crystals resulted in increased total peritoneal exudate cells (PECs) recruitment, neutrophil (CD11b<sup>+</sup>Ly6G<sup>+</sup>Ly6C<sup>lo</sup> cells) influx, and IL-1 $\beta$  release (Figures 10A-10E). These effects were more pronounced in *Gsn* <sup>$\Delta$ Mye</sup> mice, which are in agreement with my *in vitro* results (Figures 10A-10E).

The production of IL-1 $\beta$  through intraperitoneal administration of LPS is also dependent on NLRP3<sup>65</sup>. After the LPS challenge, the levels of IL-1 $\beta$  in both serum and peritoneal lavage fluid were increased in *Gsn* <sup>$\Delta$ Mye</sup> mice compared to *Gsn*<sup>fl/fl</sup> mice (Figures 11A and 11B). However, there was no significant difference in the levels of TNF $\alpha$  between the two groups in both serum and peritoneal lavage fluid (Figures 11C and 11D). Additionally, *Gsn* <sup>$\Delta$ Mye</sup> mice showed increased susceptibility to LPS-induced lethality compared to *Gsn*<sup>fl/fl</sup> mice (Figures 11E). These results further demonstrate the essential role of gelsolin in suppressing NLRP3 inflammasome-dependent inflammatory response *in vivo*.

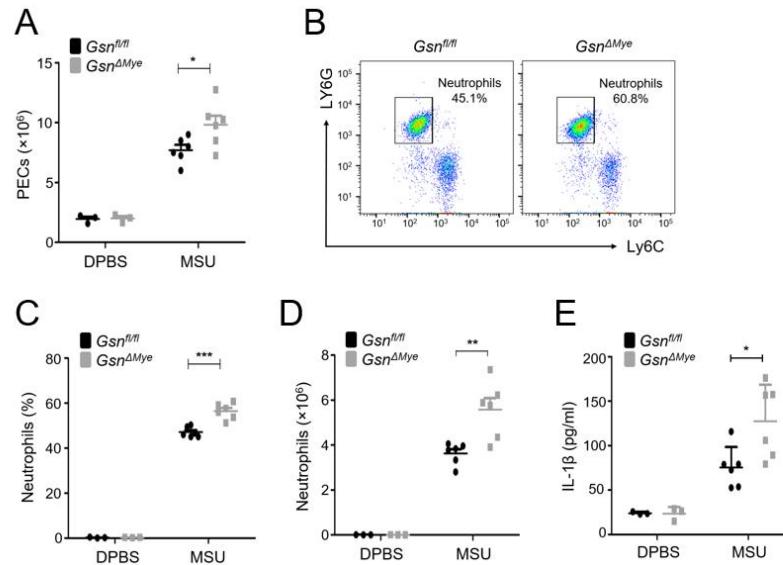


**Figure 10. Gelsolin deficiency aggravates the immunopathologic responses in the MSU-induced peritonitis model.** (A) Quantification of the total number of infiltrated PECs in *Gsn<sup>fl/fl</sup>* and *Gsn<sup>ΔMye</sup>* mice intraperitoneally injected with MSU crystals or sterile PBS. (B-D) Representative images (B), quantification of the percentage (C), and number (D) of infiltrated neutrophils (CD11b<sup>+</sup>Ly6G<sup>+</sup>Ly6C<sup>lo</sup> cells) in the peritoneal cavities of *Gsn<sup>fl/fl</sup>* and *Gsn<sup>ΔMye</sup>* mice intraperitoneally injected with MSU crystals or sterile PBS determined by flow cytometry. (E) ELISA for IL-1 $\beta$  in the peritoneal lavage fluid of *Gsn<sup>fl/fl</sup>* and *Gsn<sup>ΔMye</sup>* mice intraperitoneally injected with MSU crystals or sterile PBS. Data are presented as means  $\pm$  SEM (A, C, D) or means  $\pm$  SD (E). n = 3-6 (A-E). Student's t-test, \* $p$  < 0.05 \*\* $p$  < 0.01, \*\*\* $p$  < 0.001 (A, C-E).

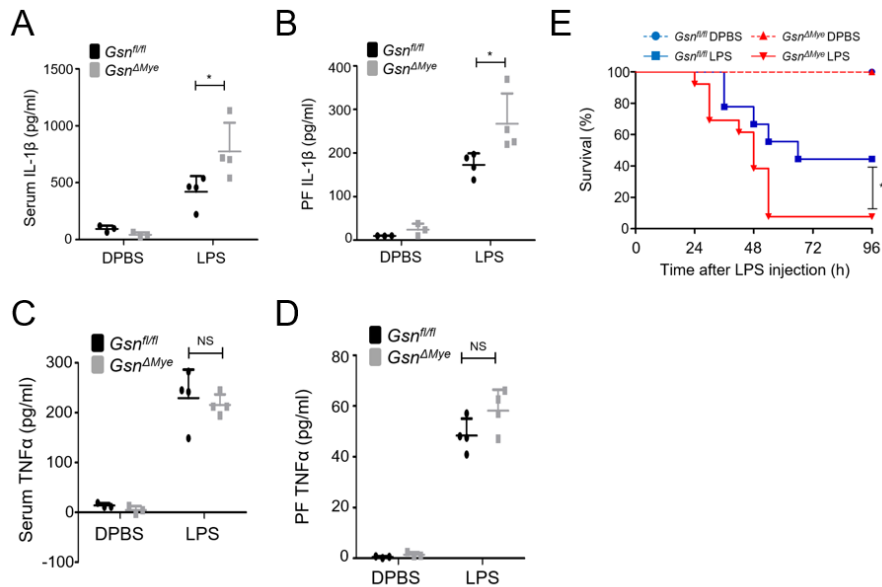


**Figure 11. Gelsolin deficiency aggravates the immunopathologic responses in the LPS-induced septic shock model.** (A-D) ELISA for serum IL-1 $\beta$  (A), peritoneal lavage fluid (PF) IL-1 $\beta$  (B), serum TNF $\alpha$  (C), peritoneal lavage fluid (PF) TNF $\alpha$  (D) of *Gsn<sup>fl/fl</sup>* and *Gsn<sup>ΔMye</sup>* mice intraperitoneally injected with 20 mg/kg LPS or sterile PBS (n = 3-4). NS, not significant. (E) Survival of *Gsn<sup>fl/fl</sup>* (n = 12) and *Gsn<sup>ΔMye</sup>* (n = 16) mice intraperitoneally injected with 10 mg/kg LPS or sterile PBS (n = 3 for each of *Gsn<sup>fl/fl</sup>* and *Gsn<sup>ΔMye</sup>*). Data are presented as means  $\pm$  SD (A-D). Student's t-test, \* $p$  < 0.05 (A-D). Log-rank test, \* $p$  < 0.05 (E).

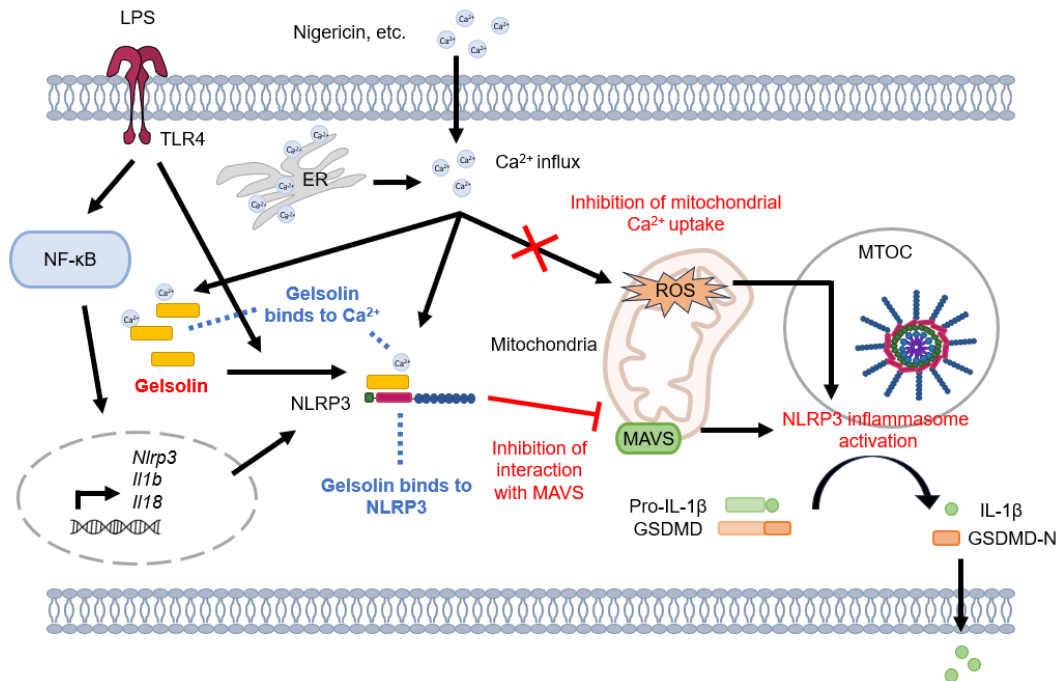


**Figure 12. A graphic summary of the mechanism of gelsolin negatively regulating NLRP3.** In LPS-primed macrophages, gelsolin interacts with NLRP3. Gelsolin inhibits the translocation of NLRP3 to the mitochondria by preventing the association between NLRP3 and MAVS. When stimulated with nigericin, the intracellular calcium concentration increases. Gelsolin helps maintain mitochondrial stability by binding to calcium and preventing mitochondrial calcium overload. Ultimately, gelsolin inhibits the activation of the NLRP3 inflammasome and pyroptosis.

## **2. Regulation of TNF $\alpha$ expression: Unveiling the role of hypersensitive site-9 enhancer RNA in *Tnf* gene control**

### **A. Downregulation of hypersensitive site-9 eRNA reduces TNF $\alpha$ expression**

To identify putative eRNAs that could potentially impact TNF $\alpha$  expression, my co-worker analyzed cap-analysis gene expression (CAGE)-seq data from the Fantom5 consortium for BMDM, and this led to the discovery of previously unannotated transcripts originating from the *Tnf* HSS-9 region. ASOs is a short nucleic acid molecule that binds to specific target transcripts, influencing gene expression by inhibiting translation or inducing degradation<sup>66</sup>. To investigate the influence of HSS-9 eRNA on TNF $\alpha$  expression, I conducted ASO-mediated HSS-9 eRNA knockdown in mouse BMDMs. Three different ASOs targeting HSS-9 eRNA were designed and transfected into BMDMs by electroporation. qRT-PCR analysis confirmed the successful decrease in the expression of the target HSS-9 eRNA following transfection with the ASOs (Figure 13). Because ASO 2 exhibited the highest efficiency among the tested ASOs, it was the only one utilized in the subsequent experiments.

Subsequently, I investigated whether alterations in the expression of HSS-9 eRNA would affect TNF $\alpha$  expression. By conducting qRT-PCR analysis, I validated that the suppression of HSS-9 eRNA resulted in a decrease in TNF $\alpha$  mRNA levels (Figure 14A). Furthermore, I also observed a reduction in the amount of TNF $\alpha$  secreted into the cell culture supernatant through ELISA (Figure 14B). These results provide evidence that modulation of HSS-9 eRNA expression directly influences TNF $\alpha$  expression at both the mRNA and protein levels.

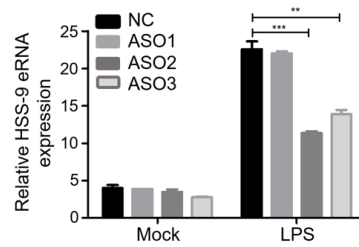


**Figure 13. ASO-mediated knockdown of HSS-9 eRNA in mouse BMDMs.** The knockdown efficiency was measured by qRT-PCR in BMDMs, left untreated and stimulated with LPS (100 ng/mL, 3 h) (n = 3). Among the three ASOs, ASO 2 significantly reduced the levels of HSS-9 eRNA. Data are presented as means  $\pm$  SEM. Student's t-test, \*\* $p < 0.01$ , \*\*\* $p < 0.001$ .

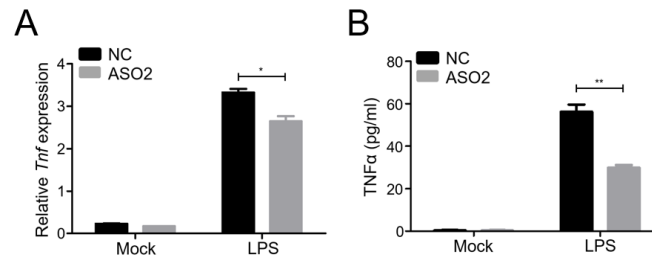


**Figure 14. Knockdown of HSS-9 eRNA reduces TNF $\alpha$  expression in macrophages.** (A) qRT-PCR analysis for mRNA expression of TNF $\alpha$  in BMDMs, left untreated and stimulated with LPS (100 ng/mL, 3 h). mRNA expression was normalized to the internal control *Gapdh* (n = 3). (B) ELISA for TNF $\alpha$  in the supernatant of BMDMs, left untreated and stimulated with LPS (100 ng/mL, 3 h) (n = 3). Data are presented as means  $\pm$  SEM. Student's t-test, \* $p$  < 0.05, \*\* $p$  < 0.01 (A, B).

### **B. Deletion of hypersensitive site-9 region reduces TNF $\alpha$ expression**

To investigate the role of HSS-9 eRNA more thoroughly, I conducted similar experiments using knockout mice with a partial deletion of the *Tnf* HSS-9 region, where HSS-9 eRNA is transcribed. These knockout mice were generated by my co-worker. First, I confirmed that in HSS-9-KO BMDMs, there is no expression of HSS-9 eRNA, in comparison to WT BMDMs (Figure 15). I discovered an approximately 50% reduction in TNF $\alpha$  mRNA and protein expression in HSS-9-KO BMDMs compared to WT BMDMs, which resulted in a clearer effect than ASOs-mediated knockdown (Figures 16A and 16C). In contrast to TNF $\alpha$ , IL-6 expression showed no significant differences (Figures 16B and 16D). These findings provide further evidence supporting the notion that HSS-9 eRNA, transcribed from the *Tnf* HSS-9 region, positively regulates TNF $\alpha$  expression.

To explore the impact of HSS-9 eRNA on positively regulating TNF $\alpha$  expression under a physiological setting, I utilized an LPS-induced septic shock model. Following the LPS challenge, there was a notable increase in TNF $\alpha$  levels observed in both serum and peritoneal lavage fluid. These effects were significantly decreased in HSS-9-KO mice (Figures 17A and 17B). However, there were no discernible differences observed in the IL-6 expression in both serum and peritoneal fluid (Figures 17C and 17D). These findings highlight the significant role of HSS-9 RNA in regulating TNF $\alpha$  expression *in vivo*.

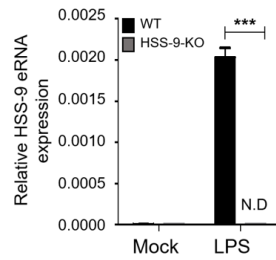


**Figure 15. No expression of HSS-9 eRNA in HSS-9-KO BMDMs.** qRT-PCR analysis for mRNA expression of TNF $\alpha$  in WT and HSS-9-KO BMDMs, left untreated and stimulated with LPS (100 ng/mL, 3 h). mRNA expression was normalized to the internal control *Gapdh* (n = 3). ND, not detected. Data are presented as means  $\pm$  SEM. Student's t-test, \*\*\* $p$  < 0.001.

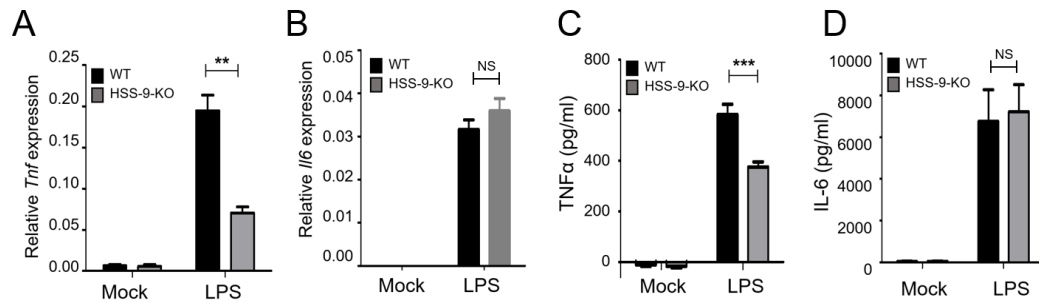


**Figure 16. Deletion of HSS-9 reduces the expression of TNF $\alpha$  in macrophages.** (A, B) qRT-PCR analysis for mRNA expression of TNF $\alpha$  (A) and IL-6 (B) in WT and HSS-9-KO BMDMs, left untreated and stimulated with LPS (100 ng/mL, 3 h). mRNA expression was normalized to the internal control *Gapdh* (n = 3). (C, D) ELISA for TNF $\alpha$  (C) and IL-6 (D) in the supernatant of WT and HSS-9-KO BMDMs, left untreated and stimulated with LPS (100 ng/mL, 3 h) (n = 3). NS, not significant. Data are presented as means  $\pm$  SEM. Student's t-test, \*\* $p$  < 0.01, \*\*\* $p$  < 0.001 (A-D).

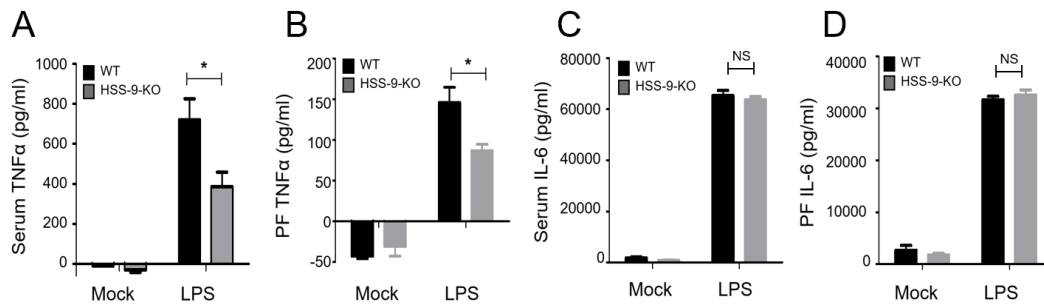


**Figure 17. Deletion of HSS-9 reduces the expression of TNF $\alpha$  in the LPS-induced septic shock model.** (A-D) ELISA for serum TNF $\alpha$  (A), peritoneal lavage fluid (PF) TNF $\alpha$  (B), serum IL-6 (C), peritoneal lavage fluid (PF) IL-6 (D) of WT and HSS-9-KO mice intraperitoneally injected with 20 mg/kg LPS or sterile PBS (n = 3-4). NS, not significant. Data are presented as means  $\pm$  SEM. Student's t-test,  $**p < 0.01$  (A-D).

### **3. Alternative role of noncoding RNAs: Involvement in tumor progression**

#### **A. Selection of antisense oligonucleotides for the precise knockdown of the eRNA *THUMPD3-AS1* and *LINC01572*, and the lncRNA *PLEKHA8P1* in HCC cell line**

To identify putative ncRNAs that influence tumor progression, several experiments were conducted by my co-workers. Two eRNAs, *THUMPD3-AS1* and *LINC01572*, were found to be commonly expressed in four different human HCC cell lines. Additionally, based on the TCGA-liver hepatocellular carcinoma (LIHC) dataset, the lncRNA *PLEKHA8P1* was discovered to be upregulated in HCC patients.

To investigate the potential significance of *THUMPD3-AS1*, *LINC01572*, and *PLEKHA8P1* in HCC cells, I performed a loss-of-function study in FT3-7, the human HCC cells line, using ASOs. Specifically, I designed one ASO to specifically target exon 3 of *THUMPD3-AS1*, another ASO to target exon 6 of *LINC01572*, and a pair of ASOs against exon 3 of *PLEKHA8P1*.

After transfecting the ASOs into FT3-7 cells, the knockdown of both *THUMPD3-AS1* and *LINC01572* was confirmed through box plots performed by a co-worker (Data not shown). Furthermore, the knockdown of *PLEKHA8P1* was confirmed through qRT-PCR analysis (Figure 18). For further investigations and analyses, only ASO 2 targeting *PLEKHA8P1* was utilized, as it showed higher effectiveness in reducing the expression level of *PLEKHA8P1* compared to the negative control.

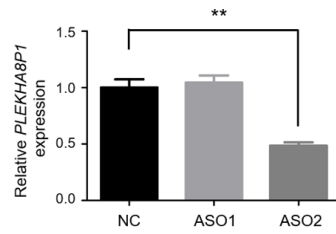


**Figure 18. ASO-mediated knockdown of *PLEKHA8P1* in HCC cells.** Knockdown efficiency was measured by qRT-PCR 48 h post-second transfection (n = 3). Between two ASOs, ASO 2 significantly reduced the levels of *PLEKHA8P1*. Data are presented as means  $\pm$  SEM. Student's t-test, \*\* $p < 0.01$ .

## **B. The eRNA *THUMPD3-AS1* and *LINC01572*, and the lncRNA**

### ***PLEKHA8P1* promotes proliferation, invasion and migration in HCC**

#### **cells**

Next, I attempted to investigate whether these three ncRNAs could promote the progression of FT3-7 cells. I observed that the knockdown of *THUMPD3-AS1*, *LINC01572* or *PLEKHA8P1* resulted in inhibited cell proliferation in proliferation assays (Figures 19A-19E). Furthermore, the colony formation assays consistently revealed a decrease of more than 40% in the number of colonies formed in the knockdown cells when compared to the control cells (Figures 19F-19I).

Because invasion and migration play a critical role in cancer metastasis<sup>67,68</sup>, I explored the impact of these ncRNAs on the invasion and migration of FT3-7 cells. The results obtained from transwell assays revealed a substantial reduction in both invasive and migratory abilities of FT3-7 cells after knockdown of *THUMPD3-AS1*, *LINC01572* or *PLEKHA8P1*, in comparison to the control group (Figures 20A-20H). Moreover, consistent findings were observed in wound-healing assays, where the ability of cells to migrate and close the induced wound was significantly impaired in the *PLEKHA8P1* knockdown group, compared to the control treatment (Figures 20I and 20J).

Collectively, these findings provide compelling evidence supporting the oncogenic roles of *THUMPD3-AS1*, *LINC01572*, and *PLEKHA8P1* in HCC cells. Their involvement in these critical processes suggests their potential as therapeutic targets for HCC treatment.

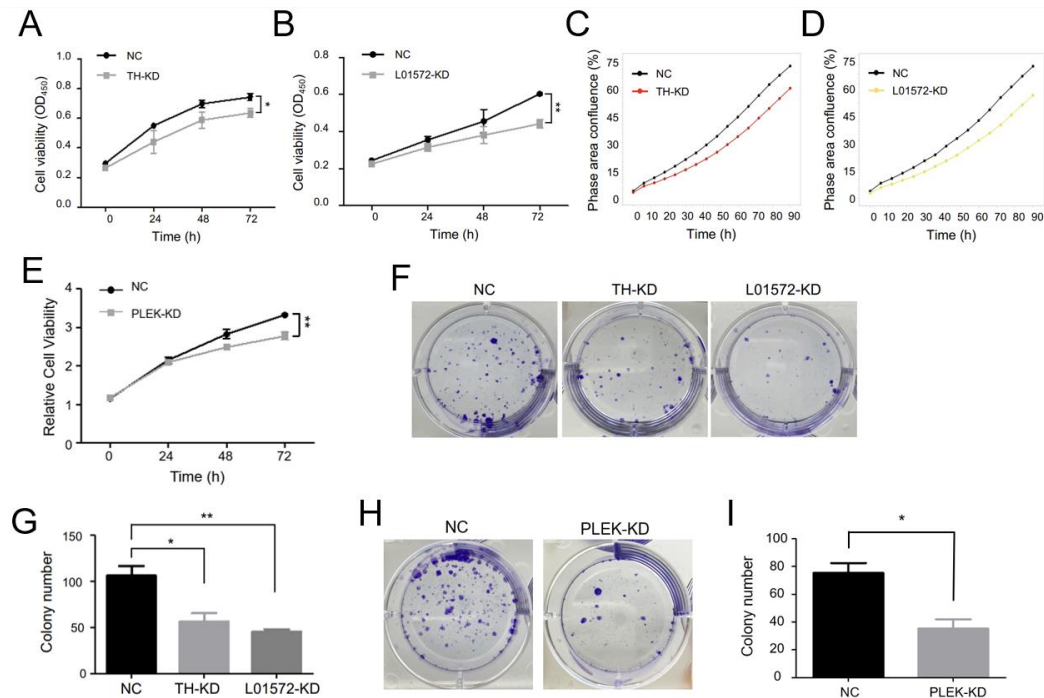


**Figure 19. Downregulation of *THUMP3-AS1*, *LINC01572* or *PLEKHA8P1* inhibits proliferation of HCC cells.** (A, B) CCK-8 assays were performed to determine cell viability at indicated time-points. OD, optical density; NC, negative control; TH-KD, *THUMP3-AS1* KD; L01572-KD, *LINC01572* KD. (C, D) IncuCyte proliferation assays were carried out to determine cell viability at the indicated times. The graph shows the mean values of technical triplicates. (E) CCK-8 assays were performed to determine cell viability at indicated time-points. OD, optical density; NC, negative control; PLEK-KD, *PLEKHA8P1* KD. (F-I) Representative images (F, H) and quantification (G, I) of colony formation assays. Data are presented as means  $\pm$  SEM (A, B, E, G, I). Student's t-test, \* $p < 0.05$ , \*\* $p < 0.01$  (A, B, E, G, I). All data are representative of at least three independent experiments.

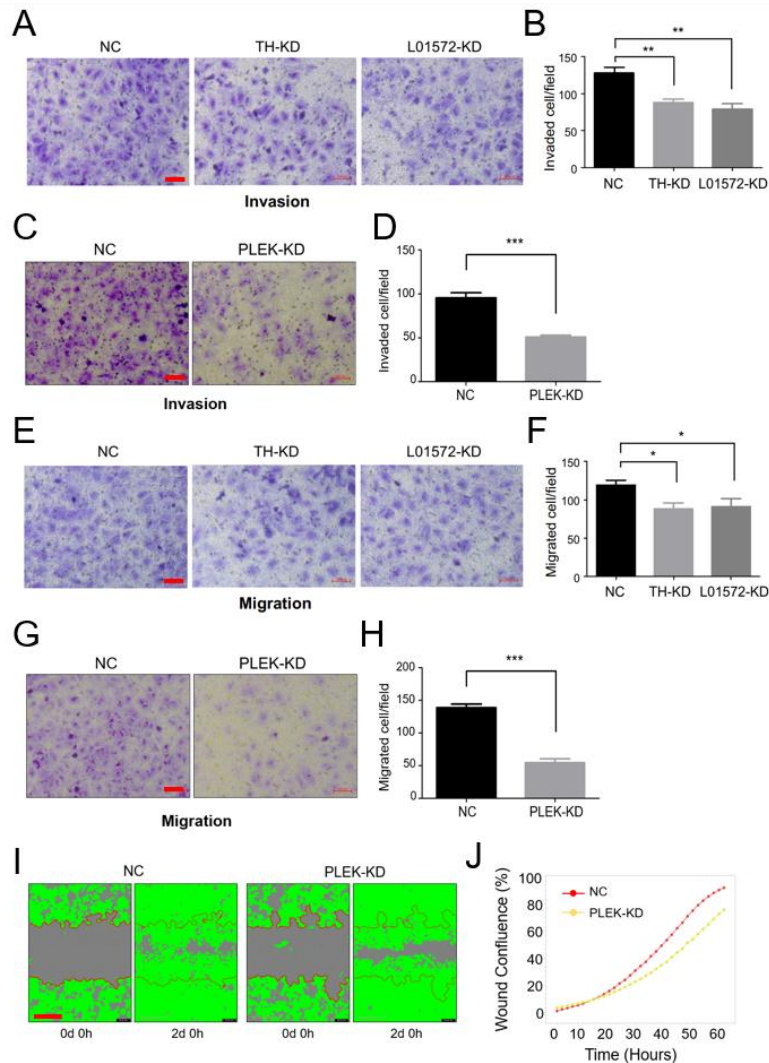


**Figure 20. Downregulation of *THUMPD3-AS1*, *LINC01572* or *PLEKHA8P1* inhibits migration and invasion of HCC cells.** (A-H) Representative images (A, C, E, G) and quantification (B, D, F, H) of transwell assays: (A-D) invasion assays and (E-H) migration assays. Scale bar, 100  $\mu$ m. (I, J) Representative images (I) and quantification (J) of wound-healing assays. The graph shows the mean values of technical triplicates. Data are presented

as means  $\pm$  SEM (B, D, F, H). Student's t-test, \* $p < 0.05$ , \*\* $p < 0.01$ , \*\*\* $p < 0.001$  (B, D, F, H). All data are representative of at least three independent experiments.

#### IV. DISCUSSION

##### 1. Regulation of IL-1 $\beta$ expression: Gelsolin-mediated negative modulation of NLRP3 inflammasome activation

The activation of NLRP3 inflammasome results in a robust innate immune response, leading to the production of active IL-1 $\beta$  and IL-18. Dysregulation of NLRP3 inflammasome activation can contribute to the development of several autoinflammatory disorders<sup>2,4</sup>. Although drugs like IL-1 receptor antagonist anakinra and anti-IL-1 $\beta$  monoclonal antibody canakinumab have been used for the treatment of autoinflammatory diseases<sup>4</sup>, blocking IL-1 $\beta$ , the central mediator of inflammation, can cause undesirable side effects. Hence, identifying a specific regulator that limits inflammasome activation may offer a better therapeutic approach.

The NLRP3 protein is initially primed by stimuli that activate NF- $\kappa$ B, such as LPS, before it forms an inflammasome complex and becomes fully activated<sup>3,4</sup>. To understand the regulatory mechanisms of NLRP3 during the priming step, my co-worker and I sought to identify its binding partner during the priming step. We discovered that gelsolin binds to NLRP3, even when only the LPS signal is given. Based on my findings in this study, it was revealed that gelsolin functions as an inhibitor of NLRP3 by restricting its activation (Figure 12). Without gelsolin, NLRP3 is more likely to be translocated to mitochondria due to increased interaction with MAVS. I observed that upon nigericin stimulation, free gelsolin, not bound to NLRP3, is translocated to the mitochondria (Figures 5A-5D). My investigation revealed that interaction of gelsolin with NLRP3 via its PYD is essential (Figure 1G), and because NLRP3 also interacts with MAVS via its PYD<sup>52</sup>, gelsolin which moves to the mitochondria may have an additional function in inhibiting the NLRP3-MAVS interaction. Furthermore, since gelsolin keeps calcium to bind with NLRP3, gelsolin-deficient macrophages exhibit higher intracellular calcium concentrations, resulting in mitochondrial damage and NLRP3 inflammasome activation. My study also demonstrated that *Gsn*<sup>ΔMye</sup> mice are more prone to MSU-induced peritonitis and LPS-

induced septic shock. Overall, these findings demonstrate a previously unknown NLRP3 inflammasome-regulatory mechanism involving gelsolin.

Gelsolin is a major actin-severing protein that depolymerizes F-actin<sup>16,17</sup>. The role of F-actin in NLRP3 inflammasome activation is being studied but still nebulous. F-actin interacts with NLRP3 and attenuates the activation of NLRP3 inflammasome through actin-binding protein Flightless-I and its binding partner LRRFIP2, known as negative modulators of NLRP3 inflammasome activation<sup>7,22,69</sup>. Latrunculin B, an actin polymerization inhibitor, reduces the amount of F-actin and promotes NLRP3 inflammasome activity<sup>69</sup>. In contrast, L-plastin, which stabilizes the formation of F-actin structures such as macrophage podosomes, promotes NLRP3 inflammasome activation by Pyk2-ASC interaction<sup>70</sup>. My discovery that gelsolin, an F-actin severing protein, negatively regulates NLRP3 inflammasome activation lends more credence to the notion that F-actin has an impact on NLRP3 inflammasome activation. However, further studies focusing on actin-severing activity of gelsolin are needed. Microtubules have been identified as mediators of NLRP3 inflammasome assembly. Recent studies have shown that NLRP3 is transported in a microtubule-dependent manner<sup>51,56,57</sup>. There is growing evidence that actin-microtubule crosstalk occurs in various mechanisms<sup>71</sup>, suggesting that actin could potentially modulate microtubule dynamics and regulate NLRP3 inflammasome activation. Further investigations could reveal the precise role of actin-microtubule interactions in NLRP3 inflammasome assembly and activation.

Previous research has shown that intracellular gelsolin is involved in various immune responses. For example, gelsolin has been shown to play a role in recruiting macrophages to damaged sites, as demonstrated by delayed recruitment of gelsolin-deficient macrophages to sciatic nerves after crush injury<sup>72</sup>. gelsolin also mediates collagen phagocytosis, as shown by reduced collagen binding in fibroblasts of gelsolin-deficient mice compared to WT mice, and this reduction was recovered by re-expression of gelsolin<sup>73</sup>. Rheumatoid arthritis, one of the chronic inflammatory diseases, is associated with the cytoskeleton reorganization activity of gelsolin<sup>20</sup>. The authors have shown that the severity

of the disease was exacerbated when gelsolin was abolished. In this paper, however, I demonstrate a novel immunological role of gelsolin in inhibiting NLRP3 inflammasome activation, and thereby, suggest a new mechanism through which gelsolin affects the pathogenesis of inflammatory diseases.

In conclusion, my findings increase the understanding of the mechanism for NLRP3 inflammasome activation, demonstrating that LPS signal primes NLRP3 and, on the one hand, facilitates the interaction between gelsolin and NLRP3 to prevent NLRP3 inflammasome activation. Additionally, I show a novel function of gelsolin, an actin-regulating protein, which affects the host immune system by modulating NLRP3 inflammasome activation. Therefore, my study provides potential avenues for the development of targeted treatments for related autoimmune diseases.

## **2. Regulation of TNF $\alpha$ expression: Unveiling the role of hypersensitive site-9 enhancer RNA in *Tnf* gene control**

It has been reported that dysregulation of eRNAs, which is transcribed by RNA pol II from enhancer regions, impacts gene regulation<sup>35,36</sup>. Consequently, the role of eRNAs in inflammatory diseases is under extensive study<sup>38</sup>.

In this study, I aimed to investigate the novel roles of HSS-9 eRNA, which is transcribed from the *Tnf* HSS-9 enhancer region and was initially identified by my co-worker. To elucidate its functions, I performed ASOs-mediated knockdown experiments. Through the knockdown of HSS-9 eRNA, I observed a significant reduction in the expression of TNF $\alpha$  mRNA and protein. Moreover, I observed a further reduction in TNF $\alpha$  expression in HSS-9-KO mice. This suggests that HSS-9 eRNA plays a crucial role in regulating the expression of TNF $\alpha$ .

While more research on detailed mechanisms is needed, based on current studies, these findings contribute to our understanding of the novel regulatory mechanism of TNF $\alpha$

regulation and may have implications for the development of therapeutic strategies targeting TNF $\alpha$ -related inflammatory disorders.

### **3. Alternative role of noncoding RNAs: Involvement in tumor progression**

Currently, it is widely acknowledged that a significant portion of the human genome is extensively transcribed into ncRNAs, and their numbers and roles in various layers of gene regulation continue to expand as research progresses. Especially, it has been reported that dysregulated expression of ncRNAs is also linked to the tumor progression<sup>40,41</sup>.

In this present study, I characterized the roles of eRNAs *THUMPD3-AS1*, *LINC01572*, and lncRNAs *PLEKHA8P1* in HCC progression. These ncRNAs were initially identified by my co-worker, and I further investigated their functions using ASOs-mediated knockdown studies. Through my experiments, I demonstrated that loss of *THUMPD3-AS1*, *LINC01572*, and *PLEKHA8P1* resulted in reduced proliferation, invasion, and migration of HCC cell line derivative FT3-7.

Since my study provides only a snapshot of the role of identified ncRNAs in tumor progression, I anticipate that additional research will be necessary to validate the current findings. Some immediate examples of future studies include utilizing more thorough perturbation techniques, such as CRISPR/Cas9 knockout of genes, to fully investigate the extent of the loss-of-function phenotype. Additionally, conducting xenograft studies will be valuable in confirming the tumorigenic role of these ncRNAs.

Nonetheless, I revealed the novel role of *THUMPD3-AS1*, *LINC01572*, and *PLEKHA8P1* in HCC cell line as oncogenic ncRNAs, highlighting their potential as promising therapeutic targets for the treatment of HCC.

## V. CONCLUSION

First, I identified a novel pathway of IL-1 $\beta$  regulation. Gelsolin binds to NLRP3 and inhibits its translocation to the mitochondria. Additionally, gelsolin keeps the calcium levels below the threshold that damages mitochondria. As a result, gelsolin inhibits NLRP3 inflammasome activation, ultimately leading to the inhibition of IL-1 $\beta$  secretion.

Second, I discovered that another important cytokine, TNF $\alpha$ , is regulated by a novel eRNA. Knockdown of the HSS-9 eRNA using ASOs or deletion of *Tnf*HSS-9 region leads to the downregulation of TNF $\alpha$  mRNA and protein expression. Notably, I confirmed a decrease in TNF $\alpha$  expression in both the serum and peritoneal fluid of the LPS-induced sepsis mouse model.

Lastly, I identified that HCC progression is regulated by novel ncRNAs. Knockdown of *THUMPD3-AS1*, *LINC01572*, and *PLEKHA8P1* using ASOs results in the downregulation of proliferation, invasion, and migration of HCC cells.

In conclusion, I uncovered novel pathways of regulation for proinflammatory cytokines IL-1 $\beta$  and TNF $\alpha$ , and additionally demonstrated that the expression of TNF $\alpha$  and tumor progression are regulated by ncRNAs. These findings suggest that targeting gelsolin, HSS-9 eRNA, *THUMPD3-AS1*, *LINC01572*, or *PLEKHA8P1* could offer promising therapeutic avenues for inflammatory diseases or HCC.

## REFERENCES

1. Broderick L, Hoffman HM. IL-1 and autoinflammatory disease: biology, pathogenesis and therapeutic targeting. *Nat Rev Rheumatol* 2022;18:448-63.
2. Schroder K, Tschopp J. The inflammasomes. *Cell* 2010;140:821-32.
3. Swanson KV, Deng M, Ting JP. The NLRP3 inflammasome: molecular activation and regulation to therapeutics. *Nat Rev Immunol* 2019;19:477-89.
4. Guo H, Callaway JB, Ting JP. Inflammasomes: mechanism of action, role in disease, and therapeutics. *Nat Med* 2015;21:677-87.
5. He Y, Hara H, Núñez G. Mechanism and regulation of NLRP3 inflammasome activation. *Trends Biochem Sci* 2016;41:1012-21.
6. Broz P, Dixit VM. Inflammasomes: mechanism of assembly, regulation and signalling. *Nat Rev Immunol* 2016;16:407-20.
7. Jin J, Yu Q, Han C, Hu X, Xu S, Wang Q, et al. LRRFIP2 negatively regulates NLRP3 inflammasome activation in macrophages by promoting Flightless-I-mediated caspase-1 inhibition. *Nat Commun* 2013;4:2075.
8. Gu P, Hui X, Zheng Q, Gao Y, Jin L, Jiang W, et al. Mitochondrial uncoupling protein 1 antagonizes atherosclerosis by blocking NLRP3 inflammasome-dependent interleukin-1 $\beta$  production. *Sci Adv* 2021;7:eabl4024.
9. Kim LK, Morita R, Kobayashi Y, Eisenbarth SC, Lee CG, Elias J, et al. AMCase is a crucial regulator of type 2 immune responses to inhaled house dust mites. *Proc Natl Acad Sci U S A* 2015;112:E2891-9.
10. Zhou R, Yazdi AS, Menu P, Tschopp J. A role for mitochondria in NLRP3 inflammasome activation. *Nature* 2011;469:221-5.

11. Heid ME, Keyel PA, Kanga C, Shiva S, Watkins SC, Salter RD. Mitochondrial reactive oxygen species induces NLRP3-dependent lysosomal damage and inflammasome activation. *J Immunol* 2013;191:5230-8.
12. Gritsenko A, Green JP, Brough D, Lopez-Castejon G. Mechanisms of NLRP3 priming in inflammaging and age related diseases. *Cytokine Growth Factor Rev* 2020;55:15-25.
13. Perri A. The NLRP3-inflammasome in health and disease. *Int J Mol Sci* 2022;23.
14. Wang Z, Zhang S, Xiao Y, Zhang W, Wu S, Qin T, et al. NLRP3 inflammasome and inflammatory diseases. *Oxid Med Cell Longev* 2020;2020:4063562.
15. Li Y, Huang H, Liu B, Zhang Y, Pan X, Yu XY, et al. Inflammasomes as therapeutic targets in human diseases. *Signal Transduct Target Ther* 2021;6:247.
16. Nag S, Larsson M, Robinson RC, Burtnick LD. Gelsolin: the tail of a molecular gymnast. *Cytoskeleton (Hoboken)* 2013;70:360-84.
17. Sun HQ, Yamamoto M, Mejillano M, Yin HL. Gelsolin, a multifunctional actin regulatory protein. *J Biol Chem* 1999;274:33179-82.
18. Piktel E, Levental I, Durnas B, Janmey PA, Bucki R. Plasma gelsolin: indicator of inflammation and its potential as a diagnostic tool and therapeutic target. *Int J Mol Sci* 2018;19.
19. Li GH, Arora PD, Chen Y, McCulloch CA, Liu P. Multifunctional roles of gelsolin in health and diseases. *Med Res Rev* 2012;32:999-1025.
20. Aidinis V, Carninci P, Armaka M, Witke W, Harokopos V, Pavelka N, et al. Cytoskeletal rearrangements in synovial fibroblasts as a novel pathophysiological determinant of modeled rheumatoid arthritis. *PLoS Genet* 2005;1:e48.

21. Antequera D, Vargas T, Ugalde C, Spuch C, Molina JA, Ferrer I, et al. Cytoplasmic gelsolin increases mitochondrial activity and reduces Abeta burden in a mouse model of Alzheimer's disease. *Neurobiol Dis* 2009;36:42-50.
22. Li J, Yin HL, Yuan J. Flightless-I regulates proinflammatory caspases by selectively modulating intracellular localization and caspase activity. *J Cell Biol* 2008;181:321-33.
23. Carpentier SJ, Ni M, Duggan JM, James RG, Cookson BT, Hamerman JA. The signaling adaptor BCAP inhibits NLRP3 and NLRC4 inflammasome activation in macrophages through interactions with Flightless-1. *Sci Signal* 2019;12.
24. Carswell EA, Old LJ, Kassel RL, Green S, Fiore N, Williamson B. An endotoxin-induced serum factor that causes necrosis of tumors. *Proc Natl Acad Sci U S A* 1975;72:3666-70.
25. Wang X, Lin Y. Tumor necrosis factor and cancer, buddies or foes? *Acta Pharmacol Sin* 2008;29:1275-88.
26. Falvo JV, Tsytsykova AV, Goldfeld AE. Transcriptional control of the TNF gene. *Curr Dir Autoimmun* 2010;11:27-60.
27. Holbrook J, Lara-Reyna S, Jarosz-Griffiths H, McDermott M. Tumour necrosis factor signalling in health and disease. *F1000Res* 2019;8.
28. Bradley JR. TNF-mediated inflammatory disease. *J Pathol* 2008;214:149-60.
29. Jang DI, Lee AH, Shin HY, Song HR, Park JH, Kang TB, et al. The role of tumor necrosis factor alpha (TNF- $\alpha$ ) in autoimmune disease and current TNF- $\alpha$  inhibitors in therapeutics. *Int J Mol Sci* 2021;22.
30. Chu WM. Tumor necrosis factor. *Cancer Lett* 2013;328:222-5.
31. Brenner D, Blaser H, Mak TW. Regulation of tumour necrosis factor signalling: live or let die. *Nat Rev Immunol* 2015;15:362-74.

32. Tsytsykova AV, Rajsbaum R, Falvo JV, Ligeiro F, Neely SR, Goldfeld AE. Activation-dependent intrachromosomal interactions formed by the TNF gene promoter and two distal enhancers. *Proc Natl Acad Sci U S A* 2007;104:16850-5.
33. De Santa F, Barozzi I, Mietton F, Ghisletti S, Polletti S, Tusi BK, et al. A large fraction of extragenic RNA pol II transcription sites overlap enhancers. *PLoS Biol* 2010;8:e1000384.
34. Kim TK, Hemberg M, Gray JM, Costa AM, Bear DM, Wu J, et al. Widespread transcription at neuronal activity-regulated enhancers. *Nature* 2010;465:182-7.
35. Arner E, Daub CO, Vitting-Seerup K, Andersson R, Lilje B, Drabløs F, et al. Transcribed enhancers lead waves of coordinated transcription in transitioning mammalian cells. *Science* 2015;347:1010-4.
36. Lam MT, Cho H, Lesch HP, Gosselin D, Heinz S, Tanaka-Oishi Y, et al. Rev-Erbs repress macrophage gene expression by inhibiting enhancer-directed transcription. *Nature* 2013;498:511-5.
37. Ye R, Cao C, Xue Y. Enhancer RNA: biogenesis, function, and regulation. *Essays Biochem* 2020;64:883-94.
38. Wan L, Li W, Meng Y, Hou Y, Chen M, Xu B. Inflammatory immune-associated eRNA: mechanisms, functions and therapeutic prospects. *Front Immunol* 2022;13:849451.
39. Yamagata K, Nakayamada S, Tanaka Y. Critical roles of super-enhancers in the pathogenesis of autoimmune diseases. *Inflamm Regen* 2020;40:16.
40. Lee JH, Xiong F, Li W. Enhancer RNAs in cancer: regulation, mechanisms and therapeutic potential. *RNA Biol* 2020;17:1550-9.
41. Guzel E, Okyay TM, Yalcinkaya B, Karacaoglu S, Gocmen M, Akcakuyu MH. Tumor suppressor and oncogenic role of long non-coding RNAs in cancer. *North Clin Istanb* 2020;7:81-6.

42. EASL Clinical Practice Guidelines: Management of hepatocellular carcinoma. *J Hepatol* 2018;69:182-236.
43. Llovet JM, Montal R, Sia D, Finn RS. Molecular therapies and precision medicine for hepatocellular carcinoma. *Nat Rev Clin Oncol* 2018;15:599-616.
44. Villanueva A. Hepatocellular carcinoma. *N Engl J Med* 2019;380:1450-62.
45. Raoul JL, Forner A, Bolondi L, Cheung TT, Kloeckner R, de Baere T. Updated use of TACE for hepatocellular carcinoma treatment: how and when to use it based on clinical evidence. *Cancer Treat Rev* 2019;72:28-36.
46. Siegel RL, Miller KD, Fuchs HE, Jemal A. Cancer statistics, 2021. *CA Cancer J Clin* 2021;71:7-33.
47. Shi H, Wang Y, Li X, Zhan X, Tang M, Fina M, et al. NLRP3 activation and mitosis are mutually exclusive events coordinated by NEK7, a new inflammasome component. *Nat Immunol* 2016;17:250-8.
48. He Y, Zeng MY, Yang D, Motro B, Núñez G. NEK7 is an essential mediator of NLRP3 activation downstream of potassium efflux. *Nature* 2016;530:354-7.
49. Guo C, Chi Z, Jiang D, Xu T, Yu W, Wang Z, et al. Cholesterol homeostatic regulator SCAP-SREBP2 integrates NLRP3 inflammasome activation and cholesterol biosynthetic signaling in macrophages. *Immunity* 2018;49:842-56.e7.
50. Bryan NB, Dorfleutner A, Rojanasakul Y, Stehlik C. Activation of inflammasomes requires intracellular redistribution of the apoptotic speck-like protein containing a caspase recruitment domain. *J Immunol* 2009;182:3173-82.
51. Misawa T, Takahama M, Kozaki T, Lee H, Zou J, Saitoh T, et al. Microtubule-driven spatial arrangement of mitochondria promotes activation of the NLRP3 inflammasome. *Nat Immunol* 2013;14:454-60.

52. Subramanian N, Natarajan K, Clatworthy MR, Wang Z, Germain RN. The adaptor MAVS promotes NLRP3 mitochondrial localization and inflammasome activation. *Cell* 2013;153:348-61.
53. Zhang Z, Meszaros G, He WT, Xu Y, de Fatima Magliarelli H, Maily L, et al. Protein kinase D at the Golgi controls NLRP3 inflammasome activation. *J Exp Med* 2017;214:2671-93.
54. Chen J, Chen ZJ. PtdIns4P on dispersed trans-Golgi network mediates NLRP3 inflammasome activation. *Nature* 2018;564:71-6.
55. Wu D, Zhang Z, Jiang X, Du Y, Zhang S, Yang XD. Inflammasome meets centrosome: understanding the emerging role of centrosome in controlling inflammasome activation. *Front Immunol* 2022;13:826106.
56. Li X, Thome S, Ma X, Amrute-Nayak M, Finigan A, Kitt L, et al. MARK4 regulates NLRP3 positioning and inflammasome activation through a microtubule-dependent mechanism. *Nat Commun* 2017;8:15986.
57. Magupalli VG, Negro R, Tian Y, Hauenstein AV, Di Caprio G, Skillern W, et al. HDAC6 mediates an aggresome-like mechanism for NLRP3 and pyrin inflammasome activation. *Science* 2020;369.
58. Elliott EI, Miller AN, Banoth B, Iyer SS, Stotland A, Weiss JP, et al. Cutting Edge: mitochondrial assembly of the NLRP3 inflammasome complex is initiated at priming. *J Immunol* 2018;200:3047-52.
59. Murakami T, Ockinger J, Yu J, Byles V, McColl A, Hofer AM, et al. Critical role for calcium mobilization in activation of the NLRP3 inflammasome. *Proc Natl Acad Sci U S A* 2012;109:11282-7.
60. Lee GS, Subramanian N, Kim AI, Aksentijevich I, Goldbach-Mansky R, Sacks DB, et al. The calcium-sensing receptor regulates the NLRP3 inflammasome through Ca<sup>2+</sup> and cAMP. *Nature* 2012;492:123-7.

61. Liu Q, Zhang D, Hu D, Zhou X, Zhou Y. The role of mitochondria in NLRP3 inflammasome activation. *Mol Immunol* 2018;103:115-24.
62. Vincent AE, Ng YS, White K, Davey T, Mannella C, Falkous G, et al. The spectrum of mitochondrial ultrastructural defects in mitochondrial myopathy. *Sci Rep* 2016;6:30610.
63. So A. Developments in the scientific and clinical understanding of gout. *Arthritis Res Ther* 2008;10:221.
64. Martinon F, Pétrilli V, Mayor A, Tardivel A, Tschopp J. Gout-associated uric acid crystals activate the NALP3 inflammasome. *Nature* 2006;440:237-41.
65. He Y, Franchi L, Núñez G. TLR agonists stimulate Nlrp3-dependent IL-1 $\beta$  production independently of the purinergic P2X7 receptor in dendritic cells and in vivo. *J Immunol* 2013;190:334-9.
66. Rinaldi C, Wood MJA. Antisense oligonucleotides: the next frontier for treatment of neurological disorders. *Nat Rev Neurol* 2018;14:9-21.
67. Lou W, Ding B, Fu P. Pseudogene-derived lncRNAs and their miRNA sponging mechanism in human cancer. *Front Cell Dev Biol* 2020;8:85.
68. Johnsson P, Morris KV, Grandér D. Pseudogenes: a novel source of trans-acting antisense RNAs. *Methods Mol Biol* 2014;1167:213-26.
69. Burger D, Fickentscher C, de Moerloose P, Brandt KJ. F-actin dampens NLRP3 inflammasome activity via Flightless-I and LRRFIP2. *Sci Rep* 2016;6:29834.
70. Joshi H, Almgren-Bell A, Anaya EP, Todd EM, Van Dyken SJ, Seth A, et al. L-plastin enhances NLRP3 inflammasome assembly and bleomycin-induced lung fibrosis. *Cell Rep* 2022;38:110507.
71. Dogterom M, Koenderink GH. Actin-microtubule crosstalk in cell biology. *Nat Rev Mol Cell Biol* 2019;20:38-54.

72. Gonçalves AF, Dias NG, Moransard M, Correia R, Pereira JA, Witke W, et al. Gelsolin is required for macrophage recruitment during remyelination of the peripheral nervous system. *Glia* 2010;58:706-15.
73. Arora PD, Glogauer M, Kapus A, Kwiatkowski DJ, McCulloch CA. Gelsolin mediates collagen phagocytosis through a rac-dependent step. *Mol Biol Cell* 2004;15:588-99.

## ABSTRACT (IN KOREAN)

**Gelsolin 및 신규 비코딩 RNAs가 전염증성 사이토카인과 종양 진행에 미치는 역할**

&lt;지도교수 김 락 균&gt;

연세대학교 대학원 의과학과

이 지 연

염증성 질환은 종종 IL-1 $\beta$  및 TNF $\alpha$  와 같은 염증성 사이토카인의 과도한 분비로 특징 지어지며, 이러한 사이토카인은 염증 반응 촉진에서 중요한 매개체로 작용한다.

IL-1 $\beta$  의 분비는 선천면역체계의 중요한 구성 요소인 NLRP3 inflammasome 에 의해 엄격히 조절된다. 본 연구에서는 NLRP3 에 결합하는 단백질인 gelsolin 을, NLRP3 inflammasome 의 활성화 및 이에 따른 IL-1 $\beta$  의 발현의 부정적 조절자로 규명했다. Gelsolin 을 녹아아웃하면 NLRP3 inflammasome 의 활성화가 현저히 증가한다. Gelsolin 은 NLRP3 의 미토콘드리아로의 이동을 방해하고 세포 내 칼슘 농도를 유지하는 데 도움을 주어 NLRP3 inflammasome 을 억제한다. 따라서 gelsolin 은 NLRP3 관련 질환의 치료를 위한 잠재적 치료 타겟이다.

추가적으로, 또 다른 중요한 사이토카인인 TNF $\alpha$  가, noncoding RNAs (ncRNAs) 클래스에 속하는 새롭게 발견된 enhancer RNA (eRNA)에 의해

조절된다는 것을 밝혔다. Hypersensitive site (HSS)-9 eRNA 를 녹다운하면 TNF $\alpha$  level 이 감소하며, HSS-9 eRNA 가 전사되는 *Tnf* HSS-9 지역을 제거하면 TNF $\alpha$  level 이 더욱 감소한다. 이러한 TNF $\alpha$  발현의 감소는 LPS 유도 패혈증 마우스 모델의 혈청 및 복막액에서 관찰되며, LPS 유도 패혈증에 대한 잠재적인 보호 효과를 시사한다. 이는 HSS-9 eRNA 가 TNF $\alpha$  관련 면역 질환을 치료하는데 유망한 치료 대상이 될 수 있음을 나타낸다.

마지막으로, 연구를 확장하여 ncRNAs 가 종양 생성에 미치는 영향을 탐구했고, *THUMPD3-AS1*, *LINC01572* 및 *PLEKHA8P1* 세 가지 ncRNAs 가 hepatocellular carcinoma (HCC)에서 종양유전자 역할을 하는 것을 밝혀냈다. 이 세 가지 ncRNAs 를 억제하면 HCC 세포의 증식, 침투 및 이동이 억제되며, 이는 이 세 가지 ncRNAs 가 HCC 치료의 잠재적 치료 타겟임을 시사한다.

이 연구는 IL-1 $\beta$  와 TNF $\alpha$  를 조절하는 새로운 메커니즘을 밝혔으며, TNF $\alpha$  발현과 종양 진행을 조절하는 ncRNAs 의 역할 또한 입증했다. 이러한 연구 결과는 염증성 질환과 HCC 를 위한 새로운 치료 전략을 제안한다.

---

핵심되는 말 : 전염증성 사이토카인, IL-1 $\beta$ , TNF $\alpha$ , gelsolin, NLRP3 inflammasome, ncRNAs, 종양 진행, antisense oligonucleotides

## PUBLICATION LIST

1. Lee YE, Lee J, Lee YS, Jang JJ, Woo H, Choi HI, et al. Identification and functional characterization of two noncoding RNAs transcribed from putative active enhancers in hepatocellular carcinoma. *Mol Cells* 2021;44:658-69.
2. Lee J, Hwang JH, Chun H, Woo W, Oh S, Choi J, et al. PLEKHA8P1 promotes tumor progression and indicates poor prognosis of liver cancer. *Int J Mol Sci* 2021;22.